Biochemistry

 Volume 18, Number 6 March 20, 1979

Picosecond Dynamics of Tyrosine Side Chains in Proteins†

J. Andrew McCammon,‡ Peter G. Wolynes, and Martin Karplus*

ABSTRACT: To probe the details of small amplitude motions in proteins, a dynamical analysis of the orientation fluctuations of two tyrosine side chains in the bovine pancreatic trypsin inhibitor is presented. Detailed results are given for the time history and correlation functions obtained for the ring motion from a molecular dynamics simulation of the entire protein. It is shown that even on a picosecond time scale orientational fluctuations of ±30° from the average position occur for the tyrosine rings in the interior of the protein. It is found that the Langevin equation is applicable to the ring torsional motion, which corresponds to that of an angular harmonic oscillator with near-critical damping. Two possible microscopic models for the observed damping effects are outlined. One of these, analogous to liquid behavior, is based on kinetic theory and takes account of the collisions which occur between atoms of the protein; the other, more analogous to solid behavior, involves the coupling among a large number of harmonic oscillators. The collisional model with parameters obtained from theoretical estimates leads to good agreement with the correlation functions from the dynamic simulation. However, the dephasing of harmonic oscillations can yield similar short-time results so that a distinction between the two models is difficult. The importance of damping effects on the motions involved in conformational transitions and enzymatic reactions is discussed.

Since the first structural data on proteins were obtained in the 1930's (Hodgkin & Riley, 1968), much effort has been devoted to identifying the specific factors which are responsible for the stability of the native conformations of these molecules. It is now possible to account for many qualitative aspects of the equilibrium structure of proteins in terms of physical principles (Richards, 1977; Chothia et al., 1977), although a detailed quantitative description is not available. That protein molecules enjoy significant internal mobility in their native states has also been recognized (Edsall, 1968; Careri et al., 1975; Weber, 1975; Cooper, 1976), and it has been suggested that the motions are of importance in the biological function of enzymes (Citri, 1973; Jencks, 1975). Nevertheless, the dynamic aspects of protein structure are still very poorly understood, and much more experimental and theoretical work is required to provide a complete picture of the nature and function of motions in proteins.

In any detailed approach to dynamic problems at the atomic level, it is essential to have available the potential energy of the system as a function of atomic coordinates. Although quantum mechanical calculations provide this for small molecules, empirical energy functions of the molecular mechanics type (Warme & Scheraga, 1974; Levitt, 1974; Gelin & Karplus, 1975) are the only possible source of such information for proteins. Since most of the motions that occur at ordinary temperatures leave the bond lengths and bond angles of the polypeptide chains near their equilibrium values, which appear not to vary significantly throughout the protein [e.g., the standard dimensions of the peptide group first proposed by Pauling, et al. (1951)], the energy function representation of the bonding can be hoped to have an accuracy on the order of that achieved in the vibrational analysis of small molecules. Where globular proteins differ from small molecules is that the contacts among nonbonded atoms play an essential role in the potential energy of the folded or native structure. From the success of the pioneering conformational studies of Ramachandran & co-workers (1963) that made use of hard-sphere nonbonded radii, it is likely that relatively simple functions (Lennard-Jones nonbonded potentials supplemented by special hydrogen-bonding terms and electrostatic interactions) can adequately describe the interactions involved.

Given such an empirical potential energy function, two types of approaches to the dynamics of the protein are possible. The first of these is static in character and can be referred to as the determination of a reaction path, in analogy to what is often done in the study of small molecules and their reactions (Schaeffer, 1972). A number of such calculations have been made recently on a variety of proteins (Gelin & Karplus, 1975; McCammon et al., 1976; Honig et al., 1976). These studies have stressed the importance of accounting for structural relaxation of the protein matrix in the calculation of conformational energy surfaces. In the case of aromatic ring rotations for the pancreatic trypsin inhibitor, for example, such

† From the Department of Chemistry, Harvard University, Cambridge, Massachusetts 02138. *Received March 27, 1978.* Supported in parts by grants from the National Science Foundation and the National Institutes of Health. J.A.M. is supported by National Institute of Health Postdoctoral Fellowship No. 1 F32 GM05717-01A1.

‡ Present address: Department of Chemistry, University of Houston, Houston, TX 77004.

0006-2960/79/0418-0927$01.00/0

adiabatic energy surfaces have been shown to yield rotation barriers which are consistent with NMR measurements, while barriers calculated for a rigid-protein matrix are much too high (Gelin & Karplus, 1975). It has been suggested also that displacement correlations due primarily to repulsion between nonbonded atoms are involved in biological function; the reaction path for tertiary structural change in hemoglobin on oxygenation is one case that has been studied in detail (Gelin & Karplus, 1977).

Thus, even from such static calculations it is clear that to determine the probability of a given structural rearrangement inside a protein, it is necessary to consider how the displacement of an individual atom is facilitated by displacement of its neighbors. It is intuitively apparent that the displacement of covalently or hydrogen-bonded atoms should be correlated; a more significant result of the recent deformation studies is that there are important correlations among the displacements of neighboring atoms even in the absence of strong bonding interactions. Such correlations among nonbonded neighbors can be rationalized in light of the dense packing of atoms inside proteins (Richards, 1977). Any bonded group of atoms in the protein interior is likely to be encaged in such a way that displacement of the group will cause overlap of the repulsive cores of group and cage atoms; thus, the displacement of the group will be energetically forbidden unless it is preceded by or concerted with an accommodating displacement of the cage atoms. The same principles are known to determine the microscopic structure and rearrangement patterns of many dense materials in the bulk (Chandler, 1974a).

The second approach to the dynamics of a protein involves solving the classical equations of motion for individual atoms with the set of forces determined from the potential function. The resulting phase space trajectories provide the ultimate detail, as well as appropriate averages, concerning the motion possible within a protein. Although small-molecule trajectory calculations (Karplus et al., 1965) and liquid-state molecular dynamics studies (Berne, 1977) are well-known, it is only recently (McCammon et al., 1977) that the equations of motion have been solved for the atoms comprising a protein. The system studied consisted of of the 454 heavy (nonhydrogen) atoms of the basic pancreatic trypsin inhibitor (BPTI) and four internal water molecules; hydrogen atoms were included implicitly by a suitable adjustment of heavy-atom parameters. The molecular dynamics calculation was based on an empirical energy function composed of a sum of terms associated with bond lengths, bond angles, dihedral angles, hydrogen bonds, and nonbonded (van der Waals and electrostatic) interactions (Gelin & Karplus, 1975); a brief description is given in Appendix A. The equations of motion were integrated for about 9 ps with an average system temperature of 295 K; the method of integration is described in Appendix B. The simulation revealed a rich variety of motional phenomena that occur on the atomic level at ordinary temperatures. Bond lengths and bond angles behaved as expected for a strongly coupled system of local oscillators that is weakly coupled to the rest of the protein molecule. By contrast, the backbone and side-chain dihedral angles, which have root mean square fluctuations between 10 and 40°, showed a relaxation behavior that appears to be dominated by interactions between nonbonded parts of the protein molecule. The individual atom fluctuations were found to have a root mean square magnitude of 0.9 Å. In many cases, the atom displacement time correlation functions show nearly monotonic decay with relaxation times of the order of a picosecond. Another feature of the dynamics was that some fragments (e.g., external side chains and amide groups) undergo transitions from one minimum to another in periods of 0.2–2 ps. Many of these changes in structure occurred smoothly, with the protein relaxing so that no large activation energy was required.

Time correlation function analyses of the local atom motions showed that dynamical information was very rapidly dissipated; that is, these motions appeared to have a "diffusional" character. This behavior is very reminiscent of what is observed in liquids and suggests that an interpretation in terms of the concepts of liquid-state theory would be appropriate. It is now known that the main dissipative mechanism in simple liquids is provided by the same hard-core forces which determine the equilibrium structure; that is, to a first approximation, the frictional properties can be related to the frequent collisions due to the hard-core interactions (Chandler, 1974a; Hynes, 1977). On the other hand, it has been traditional to describe the dynamics of isolated molecules and of solids in terms of harmonic models (Wilson et al., 1955; Maradudin et al., 1971). Moreover, it is known that the displacements of atoms in large harmonic systems can have a diffusional character over short time intervals if many normal modes contribute to the observed motion (Deutch & Silbey, 1971; Rubin, 1972; Adelman & Doll, 1977). It is therefore necessary to compare the liquidlike and solidlike dissipative mechanisms in an analysis of the frictional processes in proteins.

In this paper, we attempt to probe further the small amplitude motions that occur in proteins. For this purpose, we examine in detail the fluctuations of the aromatic ring of the relatively well-buried residue Tyr-21 in BPTI. The results are compared with those found by analyzing a previous simulation of BPTI in which a slightly different potential energy function was used (McCammon et al., 1977) and also with the results of a simulation of the dynamics of an isolated tyrosine "dipeptide" fragment. We consider primarily torsional motions of the ring, i.e., rotations about the C_{21}^{γ}–C_{21}^{ζ} axis of the vector normal to the ring plane, although significant motions of the axis itself do occur. The molecular dynamics simulation of BPTI used for the present study is very similar to the one outlined above except that a longer equilibration period (4.9 ps) preceded the 9.8-ps analysis run and small changes were made in some parameters in the energy function; the average temperature was 308 K. For the isolated tyrosine fragment simulation, the molecular model consisted of BPTI backbone atoms C_{20}^{α} through C_{22}^{α}, together with the Tyr-21 side chain. The initial coordinates for this fragment were chosen from the BPTI X-ray structure, and the backbone conformation did not vary significantly during the equilibration (1.2 ps) or analysis (9.8 ps; T = 280 K) dynamics runs. The principal conclusions of the analysis are that the torsional motions are highly damped and that the damped motions can, to a first approximation, be quantitatively described in terms of a simple Langevin equation (Chandrasekhar, 1943). It is also shown that, for short times, the damped motion is consistent with both collisional and harmonic models. Further study is required to determine which microscopic model (collisional, harmonic, or other) best describes the frictional processes associated with ring torsional motions.

In the future it is hoped to apply corresponding methods to enzyme substrate binding, enzyme catalysis, and conformational transitions where the damping can clearly play an important role. For example, it is possible to imagine situations in which an enzyme would prefer one elementary reaction step to another for purely kinetic reasons. If an enzyme had several possible reaction paths, the dominant contribution might be

FIGURE 1: Disposition of the Tyr-21 residue and selected neighboring atoms in the X-ray structure. Neighboring atoms include the backbone atoms of residues 30–32 and 45–48 (α carbons are numbered) and the side chain of Thr-32 (shaded). The rigid-protein torsional potential for the X-ray structure (E_R in Figure 3) arises primarily from $C_{21}{}^{\epsilon 2}$ to $C_{32}{}^{\gamma 2}$ repulsion for positive torsions and from $C_{21}{}^{\delta 1}$ to N_{21} and (to a lesser extent) $C_{21}{}^{\delta 1}$ to $C_{21}{}^{\alpha}$ repulsions for negative torsions.

from the one in which structural relaxations were attended by the least internal friction. Such a pathway could become available before others with lower effective barriers if the relaxation times were long relative to the reaction rate. There is also the possibility that the energy liberated in substrate binding might not be dissipated before it can be utilized for the enzymatic reaction. Moreover, it is known that frictional effects can be important in affecting the character of the transition which does occur, determining in some cases the length of time a system spends near the top of an energy barrier (Kramers, 1940). Frictional effects are important also in providing the means whereby dynamical information is dissipated in a structural transition, locking the protein into its new conformational state.

The molecular dynamics results are outlined under Molecular Dynamics Results; the potential function and calculational method are described in Appendices A and B, respectively. The structural aspects and magnitude of the ring motion are examined and it is shown that the fluctuations are larger than those predicted in a rigid protein. The results for Tyr-21 in BPTI are compared also with those obtained from the molecular dynamics calculation on the isolated tyrosine fragment, in which effects due to the surrounding protein matrix are absent. To describe the details of the ring motion, time correlation functions for the torsional displacement, the squared torsional displacement and the torsional angular velocity are presented. The Phenomenological Analysis of Ring Motion section uses the Langevin equation to provide a phenomenological analysis of the calculated ring motion. In the Microscopic Models for the Friction section, the observed correlation functions for the tyrosine ring are compared with predictions based on collisional and harmonic models. The results and analysis are discussed in the Discussion section.

Molecular Dynamics Results

In the native conformation of BPTI, the Tyr-21 ring is surrounded by and has significant nonbonded interactions with atoms in its own backbone and in residues 30, 31, 32, 45, 47, and 48. The disposition of the ring and its neighbors in the X-ray structure is shown in Figure 1 (Huber et al., 1970; Deisenhofer & Steigemann, 1975). The ring exhibits substantial orientational fluctuations, but no complete rotational transitions are observed during the 9.8-ps dynamical simulation. Tyr-35 was also studied; since its small amplitude torsional motions were found to be very similar to those of Tyr-21, detailed results are quoted only for the latter.

To quantitatively describe these orientational fluctuations, a set of coordinate axes was fixed to the ring: the unit vector $\mathbf{e}_x$ was defined as the normal to the best plane through the ring atoms (Schomaker et al., 1959), the unit vector $\mathbf{e}_z$ was chosen

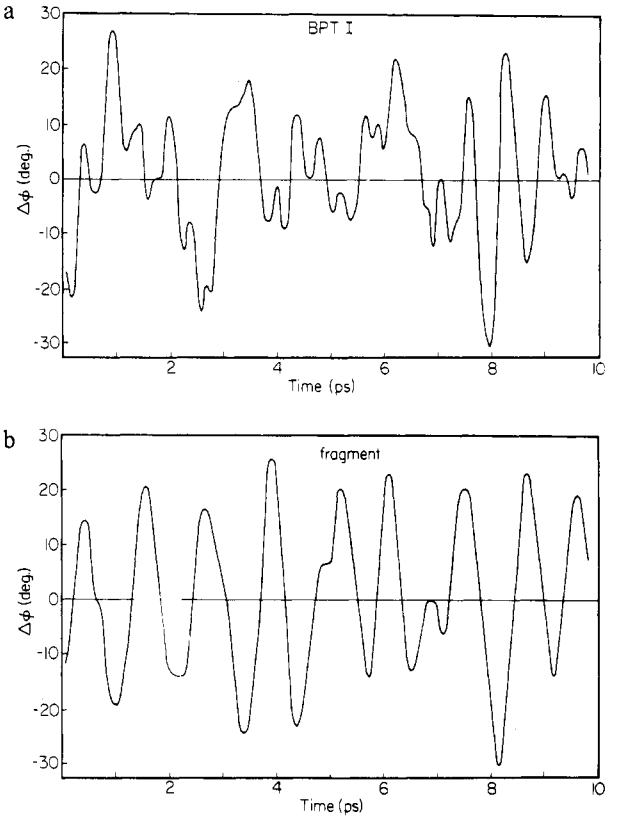

FIGURE 2: (a) Evolution of the Tyr-21 ring torsional angle during the 9.8 ps of dynamical simulation in the protein. (b) Evolution of the tyrosine ring torsional angle during 9.8 ps of dynamical simulation on the isolated tyrosine fragment.

in the $C_{21}{}^{\gamma}$ to $C_{21}{}^{\zeta}$ direction, and $\mathbf{e}_y$ was defined as the cross product ($\mathbf{e}_z \times \mathbf{e}_x$). Comparing one coordinate set from the dynamical simulation with the previous coordinate set, the increment in torsion angle was defined as arcsin ($\mathbf{e}_x \times \mathbf{e}_y'$), where the prime refers to the earlier coordinate set. Increments of the torsion axis $\mathbf{e}_z$ itself were defined as arcsin ($\mathbf{e}_x \times \mathbf{e}_z'$) for the displacements in a plane perpendicular to the ring and as arcsin ($\mathbf{e}_z \times \mathbf{e}_y'$) for the displacements in the plane of the ring. The ring-fixed axes were chosen so that positive torsional increments correspond to positive increments of the dihedral angle $\chi_{21}{}^2$; the present description of the torsional displacements is preferred to the use of $\chi_{21}{}^2$ since this dihedral angle is sensitive to local atomic motions (e.g., oscillations of the side chain atom $C_{21}{}^{\beta}$) as well as to actual ring reorientations.

Summation of the torsional increments obtained for Tyr-21 during the BPTI simulation yields the net torsional fluctuation history shown in Figure 2a; the quantity plotted is $\Delta\phi = \phi - \langle\phi\rangle$, where $\langle\phi\rangle$ is the time average of the net torsion. The effects of the local atomic motions on $\chi_{21}{}^2$ should tend to vanish in time averaging, so we can roughly associate $\langle\phi\rangle$ with the dynamical average $\langle\chi_{21}{}^2\rangle \simeq 90°$. The corresponding torsional fluctuation history for the ring in the isolated tyrosine fragment simulation is shown in Figure 2b. Comparison of the two figures shows that the torsional motion of the ring is less regular when it is surrounded by the protein matrix than in the separated fragment. In BPTI, the root mean square fluctuation of the Tyr-21 torsion angle is 12°, while root mean square fluctuations of the torsion axis are 9° (in the plane of the ring) and 38° (in a plane perpendicular to the ring). For Tyr-35, the corresponding root mean square fluctuations were 12, 9, and 11°, respectively. The motion of the Tyr-21 torsion axis in a plane perpendicular to the ring is dominated by a steady drift over the course of the simulation; examination of

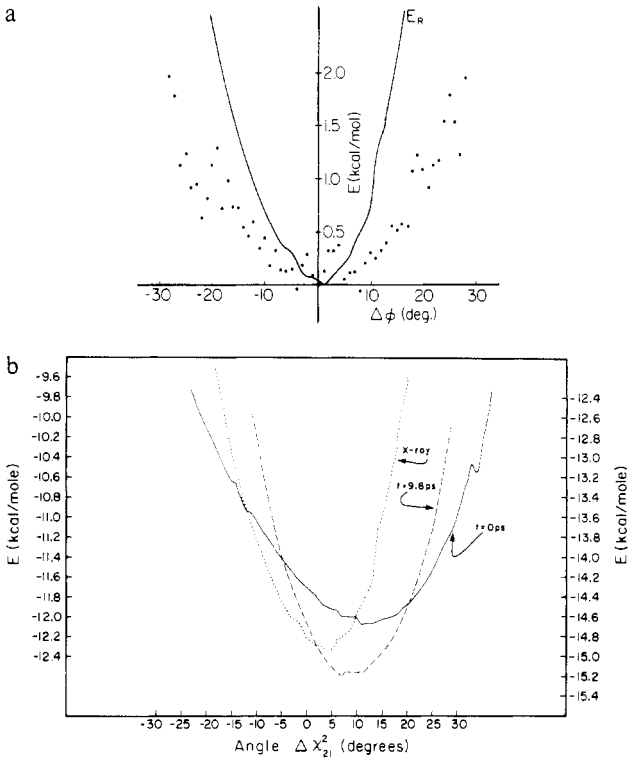

FIGURE 3: (a) Points representing the potential of mean force for Tyr-21 ring torsional fluctuations, based on statistics from the dynamical simulation. E_R is the total potential energy for Tyr-21 ring torsional displacements in the rigid X-ray structure. (b) Comparison of rigid rotation curves for Tyr-21 ring for three geometries; (···) X-ray, (—) t = 0 ps; (– – –) t = 9.8 ps. The origin (0°) in each case corresponds to the $\chi_{21}{}^2$ angle of the coordinate set. The energy scale on the left is associated with the X-ray and t = 0 ps results while that on the right is for t = 9.8 ps; the values correspond to the interaction energy of the tyrosine ring and the rest of the protein.

successive coordinate sets and comparison with the previous simulation of BPTI (in which no such drift occurred) suggest that this drift reflects a slow collective fluctuation of the ring and its surroundings. The average root mean square displacement of the Tyr-21 side chain atoms is 0.7 Å. For the isolated tyrosine fragment, the root mean square fluctuation of the torsion angle is 15°, the root mean square fluctuations of the torsion axis are 6° in both directions, and the average root mean square displacement of the side chain atoms is 0.25 Å.

The free energy of a torsional fluctuation of the Tyr-21 ring is given by the potential of mean force (Hill, 1960)

$$E(\Delta\phi) = -RT \ln \rho(\Delta\phi) \qquad (1)$$

where $\rho(\Delta\phi)$ is the relative likelihood of a fluctuation, $\Delta\phi$, of ϕ from its average value, $\langle\phi\rangle$, R is the gas constant, T is the absolute temperature, and $\rho(0)$ is normalized to 1. The quantity $\rho(\Delta\phi)$ was obtained from the BPTI simulation by calculating $\Delta\phi$ at each of 2000 equally spaced times and displaying the results as a histogram with torsional intervals of 1°. The resulting potential of mean force is shown in Figure 3a. For purposes of comparison we also show in Figure 3a a potential, $E_R(\Delta\phi)$, whose shape is determined by rotating the Tyr-21 ring in the rigid X-ray structure. Rotation of the Tyr-21 ring in other rigid coordinate sets selected from the dynamical simulation yields curves of somewhat different shapes, depending on the positions of the cage atoms. The energy $E_R(\Delta\phi)$ is almost entirely due to repulsive van der Waals contacts between a few atoms in the ring and a few atoms in the cage (cf. Gelin & Karplus, 1975). This is also true for the rigid rotation curves calculated using other coordinate sets from the simulation, although different atoms are involved as the dynamics progresses. To illustrate this, we show in Table I the important interactions for the X-ray geometry and two other geometries from the dynamics run; the first corresponds to the beginning of the simulation after the equilibration period (t = 0 ps) and the second to the end of the simulation (9.8 ps). For each geometry, the origin (0°) is chosen to be that corresponding to the calculated ring orientation and rigid rotation results to ±40° are listed. As indicated in the footnote to the table, the origin is in the neighborhood of the rigid rotation minimum but not identical with it (±10°); in the standard convention, the values of $\chi_{21}{}^2$ are all near 90°, as expected. Only the contributions which depend on the torsional angle are included; interactions that are large but independent of angle (e.g., $C_{21}{}^{\gamma}$ with $C_{21}{}^{\zeta}$) are omitted. Because the electrostatic potential varies slowly with distance and there are no charged groups involved, only the van der Waals terms play a role; that is, the significant interactions arise from short nonbonded contacts. It can be seen that in some cases important terms arise from contacts between the tyrosine ring and its own main chain atoms; e.g., for negative rotations in the X-ray geometry, $C_{21}{}^{\delta 1}$ interacts strongly with $C_{21}{}^{\alpha}$ and N_{21} (see Figure 1). Such terms are included in the fragment simulation. The local main chain interactions are relatively less important in the two other geometries (t = 0, 9.8 ps) for negative rotations and are negligible for positive rotations in all geometries. The dominant repulsions contributing to the potential curve from residues at a distance from Tyr-21 along the main chain come from Thr-32 for both positive and negative rotations, Ser-47 plus Cys-30 for positive rotation, and Ala-48 for negative rotation (Figure 1). Although the same residues tend to contribute in all three geometries, the magnitude of their contributions and the particular atoms involved are different. Thus, for example, while it is the $C^{\gamma 2}$ of Thr-32 interacting with $C_{21}{}^{\epsilon 1}$ that is important for negative twists in the X-ray and t = 0 geometries, in the t = 9.8-ps geometry, it is $O^{\gamma 1}$ and C^{β} of Thr-32 interacting with both $C_{21}{}^{\epsilon 1}$ and $C_{21}{}^{\delta 1}$ that dominate. Similarly, it is the carbonyl carbon of Ser-47 which contributes for the X-ray and t = 0 ps geometries (positive rotations), while the carbonyl oxygen is more important in the t = 9.8-ps geometry. Also, the carbonyl oxygen of Cys-30 plays no role in the X-ray and t = 9.8-ps structures but is significant (positive rotations) for the t = 0-ps geometry. Of interest is the fact that its repulsive contribution is not monotonic with angle since it increases up to 20° and then decreases again; apparently the ring $C_{21}{}^{\delta 2}$ atom passes by O_{30} as it undergoes a positive rotation.

For the various geometries, the rigid rotation curves are shown in Figure 3b; the origins for these curves are defined as in Table I. Even though there are a small number and sometimes different nonbonded (R^{-12}) interactions contributing at the various angles, the energy curves show a relatively smooth angular dependence. The three curves are significantly different in form but in all cases have nonnegligible anharmonic contributions over the range of interest. Some very short nonbonded contacts and correspondingly high repulsive energies result from the rigid rotations (e.g., 23.2 kcal from $C_{21}{}^{\epsilon 1}$ to $O_{32}{}^{\gamma 1}$ in the t = 9.8-ps geometry for −40°). Clearly, such contacts do not occur in the actual dynamic simulation; that is, the ring would only rotate to −40° if $O_{32}{}^{\gamma 1}$ had moved sufficiently to decrease the repulsive interaction to a value on the order of k_BT. This important point is reinforced by Figure 3a which shows that the potential of mean force, $E(\Delta\phi)$, is significantly softer than the rigid-protein potential, $E_R(\Delta\phi)$.

Table I: Dominant Nonbonded Interactions in Tyr-21 Rigid Rotation Potentials for Several BPTI Coordinate Sets[a,b]

ring	other[a]	distance (Å)	energy (kcal/mol)
	A. X-ray Structure		
	Twist = −40°		
$C^{\epsilon 2}$	C^{β} (Ala-48)	2.99	2.68
$C^{\delta 1}$	C^{α} (Tyr-21)	2.91	1.97
$C^{\delta 2}$	C^{α} (Ala-48)	2.93	1.76
$C^{\delta 1}$	N (Tyr-21)	2.84	1.74
$C^{\epsilon 1}$	$C^{\gamma 2}$ (Thr-32)	3.12	1.21
$C^{\delta 2}$	C^{β} (Ala-48)	3.20	0.71
$C^{\delta 1}$	C (Arg-20)	3.07	0.66
$C^{\delta 2}$	N (Ala-48)	3.04	0.36
	Twist = −30°		
$C^{\delta 1}$	N (Tyr-21)	2.87	1.46
$C^{\delta 1}$	C^{α} (Tyr-21)	2.98	1.31
$C^{\epsilon 2}$	C^{β} (Ala-48)	3.11	1.26
$C^{\delta 2}$	C^{α} (Ala-48)	3.10	0.60
$C^{\delta 1}$	C (Arg-20)	3.15	0.35
	Twist = −20°		
$C^{\delta 1}$	N (Tyr-21)	2.92	0.97
$C^{\delta 1}$	C^{α} (Tyr-21)	3.06	0.79
$C^{\epsilon 2}$	C^{β} (Ala-48)	3.27	0.39
	Twist = −10°		
$C^{\delta 1}$	N (Tyr-21)	3.01	0.48
$C^{\delta 1}$	C^{α} (Tyr-21)	3.15	0.41
	Twist = 0°		
	none with energy > 0.3 kcal/mol		
	Twist = +10°		
$C^{\epsilon 2}$	$C^{\gamma 2}$ (Thr-32)	3.30	0.31
	Twist = +20°		
$C^{\epsilon 2}$	$C^{\gamma 2}$ (Thr-32)	3.10	1.39
$C^{\delta 1}$	C (Ser-47)	3.11	0.50
	Twist = +30°		
$C^{\epsilon 2}$	$C^{\gamma 2}$ (Thr-32)	2.91	4.02
$C^{\delta 1}$	C (Ser-47)	2.92	1.87
$C^{\delta 1}$	N (Ala-48)	2.98	0.65
$C^{\delta 1}$	C^{α} (Ser-47)	3.14	0.45
	Twist = +40°		
$C^{\epsilon 2}$	$C^{\gamma 2}$ (Thr-32)	2.74	9.69
$C^{\delta 1}$	C (Ser-47)	2.75	4.78
$C^{\delta 1}$	N (Ala-48)	2.77	2.68
$C^{\epsilon 1}$	N (Ala-48)	2.93	0.94
$C^{\delta 1}$	C^{α} (Ser-47)	3.06	0.83
$C^{\delta 2}$	C^{α} (Tyr-21)	3.13	0.48
$C^{\delta 2}$	$C^{\gamma 2}$ (Thr-32)	3.29	0.32
	B. Initial Dynamics Structure (t = 0 ps)		
	Twist = −40°		
$C^{\delta 1}$	C^{α} (Tyr-21)	2.83	3.15
$C^{\epsilon 1}$	$C^{\gamma 2}$ (Thr-32)	2.99	2.63
$C^{\epsilon 2}$	C^{α} (Ala-48)	3.14	0.45
$C^{\delta 1}$	N (Tyr-21)	3.02	0.41
	Twist = −30°		
$C^{\delta 1}$	C^{α} (Tyr-21)	2.86	2.76
$C^{\epsilon 1}$	$C^{\gamma 2}$ (Thr-32)	3.13	1.12
$C^{\delta 1}$	N (Tyr-21)	2.98	0.63
	Twist = −20°		
$C^{\delta 1}$	C^{α} (Tyr-21)	2.90	2.20
$C^{\delta 1}$	N (Tyr-21)	2.96	0.73
	Twist = −10°		
$C^{\delta 1}$	C^{α} (Tyr-21)	2.95	1.61
$C^{\delta 1}$	N (Tyr-21)	2.98	0.65
	Twist = 0°		
$C^{\delta 1}$	C^{α} (Tyr-21)	3.02	1.07
$C^{\delta 1}$	N (Tyr-21)	3.02	0.43
$C^{\delta 2}$	O (Cys-30)	2.95	0.40
	Twist = +10°		
$C^{\delta 2}$	O (Cys-30)	2.85	0.85
$C^{\delta 1}$	C^{α} (Tyr-21)	3.09	0.64
	Twist = +20°		
$C^{\delta 2}$	O (Cys-30)	2.81	1.16
$C^{\delta 1}$	C^{α} (Tyr-21)	3.17	0.34
$C^{\delta 2}$	C (Cys-30)	3.15	0.33
	Twist = +30°		
$C^{\delta 2}$	O (Cys-30)	2.82	1.10
$C^{\epsilon 1}$	C^{α} (Ser-47)	3.14	0.45
$C^{\epsilon 1}$	C (Ser-47)	3.14	0.39
$C^{\delta 1}$	C (Ser-47)	3.14	0.37
	Twist = +40°		
$C^{\epsilon 1}$	C (Ser-47)	2.94	1.65
$C^{\delta 1}$	C (Ser-47)	2.99	1.22
$C^{\epsilon 1}$	C^{α} (Ser-47)	3.00	1.15
$C^{\delta 2}$	O (Cys-30)	2.88	0.72
$C^{\epsilon 1}$	N (Ala-48)	3.04	0.33
	C. Final Dynamics Structure (t = 9.8 ps)		
	Twist = −40°		
$C^{\epsilon 1}$	$O^{\gamma 1}$ (Thr-32)	2.39	23.16
$C^{\epsilon 1}$	C^{β} (Thr-32)	2.66	7.80
$C^{\delta 1}$	$O^{\gamma 1}$ (Thr-32)	2.67	5.04
$C^{\delta 1}$	C^{β} (Thr-32)	2.92	1.88
$C^{\delta 1}$	C^{α} (Tyr-21)	3.02	1.06
$C^{\delta 1}$	N (Tyr-21)	2.93	0.92
$C^{\epsilon 2}$	N (Ala-48)	2.97	0.69
$C^{\delta 2}$	N (Ala-48)	2.99	0.55
$C^{\epsilon 2}$	C^{β} (Ala-48)	3.25	0.47
	Twist = −30°		
$C^{\epsilon 1}$	$O^{\gamma 1}$ (Thr-32)	2.56	9.34
$C^{\epsilon 1}$	C^{β} (Thr-32)	2.87	2.50
$C^{\delta 1}$	$O^{\gamma 1}$ (Thr-32)	2.82	2.09
$C^{\delta 1}$	N (Tyr-21)	2.94	0.86
$C^{\delta 1}$	C^{α} (Tyr-21)	3.07	0.75
$C^{\delta 1}$	C^{β} (Thr-32)	3.12	0.54
	Twist = −20°		
$C^{\epsilon 1}$	$O^{\gamma 1}$ (Thr-32)	2.75	3.21
$C^{\epsilon 1}$	C^{β} (Thr-32)	3.09	0.67
$C^{\delta 1}$	$O^{\gamma 1}$ (Thr-32)	2.99	0.64
$C^{\delta 1}$	N (Tyr-21)	2.98	0.63
$C^{\delta 1}$	C^{α} (Tyr-21)	3.13	0.48
	Twist = −10°		
$C^{\epsilon 1}$	$O^{\gamma 1}$ (Thr-32)	2.95	0.87
$C^{\delta 1}$	N (Tyr-21)	3.04	0.33
	Twist = 0°		
	none with energy > 0.3 kcal/mol		
	Twist = +10°		
	none with energy > 0.3 kcal/mol		
	Twist = +20°		
	none with energy > 0.3 kcal/mol		
	Twist = +30°		
$C^{\delta 1}$	O (Ser-47)	2.86	0.78
$C^{\epsilon 2}$	C^{β} (Thr-32)	3.07	0.77
$C^{\delta 1}$	C (Ser-47)	3.12	0.47
	Twist = +40°		
$C^{\epsilon 2}$	C^{β} (Thr-32)	2.85	2.90
$C^{\delta 1}$	O (Ser-47)	2.72	2.04
$C^{\delta 1}$	C (Ser-47)	2.96	1.47
$C^{\delta 2}$	C^{β} (Thr-32)	3.06	0.79

[a] All atoms whose contribution to the torsional potential is greater than 0.3 kcal are listed. [b] The reference twist angle (twist = $\Delta\chi_{21}^{2} = 0°$) is the one that occurs in the given structure; it is near but not at the potential energy minimum (the minima are X-ray, 4°; t = 0 ps, 11°; t = 9.8 ps, 7°; in the conventional description, these dihedral angles are χ_{21}^{2} = 80, 60, and 77°, respectively).

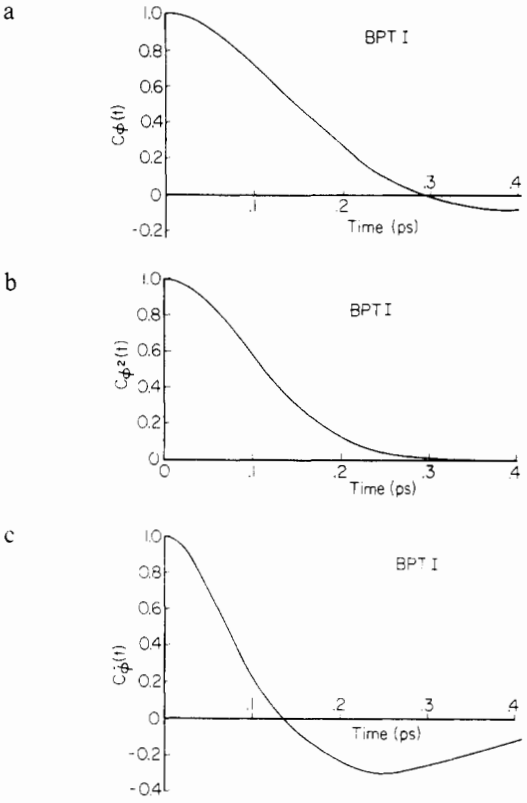

FIGURE 4: (a) The normalized time correlation function for torsional fluctuations of the Tyr-21 ring, based on molecular dynamics results. (b) The normalized time correlation function for squared torsional fluctuations of the Tyr-21 ring, based on molecular dynamics results. (c) The normalized time correlation function for the torsional angular velocity of the Tyr-21 ring, based on molecular dynamics results.

Correlations in the displacements of ring and cage atoms in the fluctuating protein tend to lower the energy required for a given displacement. Such correlations are also manifest in the fact that the rigid rotation curves calculated using coordinates from the simulation have minima which vary over a range of roughly ±10° from $\langle\phi\rangle$. Thus, an estimate of the typical cage atom displacements which contribute to the softening of the potential of mean force is 0.2 Å, the distance a δ or ϵ ring carbon moves upon a 10° torsional rotation.

Time Correlation Functions. In the analysis of the dynamic character of structural fluctuations in a protein, it is useful to introduce time correlation functions (Zwanzig, 1965). The time correlation function, $C_A(t) = \langle A(s + t)A(s)\rangle$, for a dynamical variable A is obtained by multiplying the value of $A(s)$ by $A(s + t)$, the value taken by A after the system has evolved for an additional time t, calculating such products for a representative set of initial times, s, and averaging. If the averaging is done over a sufficiently long dynamical simulation of an equilibrated system, $C_A(t)$ will be independent of the initial times, s, used in the calculation; it is then customary to write $C_A(t) = \langle A(t)A(0)\rangle$. If A is the fluctuation of a variable from its mean value, $\langle[A(0)]^2\rangle$ is the mean-square fluctuation of the variable for an equilibrated system, while the time correlation function, $C_A(t)$, describes the average way in which the fluctuation decays. In this section we present several molecular dynamics time correlation functions relating to the torsional motions of the Tyr-21 ring in BPTI and in the fragment.

The normalized time correlation function for torsional fluctuations of the Tyr-21 ring in BPTI, $C_\phi(t) = \langle\Delta\phi(t)\Delta\phi(0)\rangle/\langle[\Delta\phi(0)]^2\rangle$, is shown in Figure 4a. It is clear that the torsional oscillations of the ring are significantly damped. To more fully characterize the manner in which torsional fluctuations relax, we present in Figure 4b the normalized time correlation function for the square of the torsional fluctuation, $C_{\phi^2}(t) = \langle\Delta\phi^2(t)\Delta\phi^2(0)\rangle/\langle[\Delta\phi^2(0)]^2\rangle$. The introduction of this function is motivated by the successful use of time correlation functions for the Legendre polynomials of order l = 1 and l = 2 in the analysis of reorientational motions in fluids; comparing the decay times for such functions can help to discriminate between small-step and large-step diffusional processes, for example (Berne & Pecora, 1976). In Figure 4c we present the normalized time correlation function for the torsional angular velocity, $C_{\dot\phi}(t) = \langle\dot\phi(t)\dot\phi(0)\rangle/\langle[\dot\phi(0)]^2\rangle$. The error theory of Zwanzig & Ailawadi (1969) indicates that these functions may not be quantitatively reliable for times greater than about 0.2 ps; that is, determination of the exact behavior of the correlation functions in the region where they are small (i.e., after their initial decay) would require a longer simulation study. Nevertheless, it is apparent that the functions are strongly damped, in contrast to the continued oscillation expected for an isolated harmonic oscillator.

In Figures 5a,b, we present for comparison the plots of $C_\phi(t)$ and $C_{\phi^2}(t)$ calculated from the dynamical simulation of the isolated tyrosine fragment. It is apparent that the tyrosine ring suffers substantially less damping during its torsional motion in the isolated fragment than in intact BPTI. $C_\phi(t)$ and $C_{\phi^2}(t)$ both exhibit longer decay times and more oscillatory character in the tyrosine fragment.

Phenomenological Analysis of Ring Motion

In this section, we seek to characterize in a general way the physical processes underlying the tyrosine ring torsional fluctuations in BPTI. The inquiry is limited to the estimation of the relative importance of inertial and frictional effects and to some consideration of the time scales of the processes involved. We begin by assuming that the torsional motion of the Tyr-21 ring is described by the Langevin equation for the harmonic oscillator (Chandrasekhar, 1943),

$$I\ddot\phi + f\dot\phi + k\phi = N_r(t) \qquad (2)$$

Here ϕ is the torsional coordinate relative to $\langle\phi\rangle = 0$, I = 7.5 × 10^{-15} g cm^2 mol^{-1} is the moment of inertia of the ring about the $C_{21}{}^{\gamma}$–$C_{21}{}^{\zeta}$ axis, f is a friction constant, k is the harmonic restoring force constant, and $N_r(t)$ represents the random torques acting on the ring due to fluctuations in its environment. In using a Langevin equation, we implicitly assume that variations in $N_r(t)$ occur on a much shorter time scale than do variations in ϕ; thus, $N_r(t)$ may be regarded as a Gaussian random process and we do not have to specify the mechanism by which the torque fluctuations arise. This time scale assumption is supported by the collisional model argument in the next section; it is shown there that the mean time between significant changes in $N_r(t)$ is about 0.07 ps; reference to Figure 4 shows that, on the average, ϕ does not change much in this short interval of time. The form of the correlation function in the Langevin model is (Appendix C)

$$C_\phi{}^{L}(t) = e^{-\beta t/2}\left[\cos at + \left(\frac{\beta}{2a}\right)\sin at\right] \qquad (3)$$

where β and a are defined in Appendix C.

For the restoring force constant, k, it is appropriate to choose a value that includes the effects of cage relaxation. A quadratic fit to the potential of mean force, $E(\Delta\phi)$, defined in eq 1 yields for Tyr-21 the force constant k = 5.5 × 10^{11} erg rad^{-2} mol^{-1}; the rigid-protein force constant is k = 2.2 × 10^{12} erg rad^{-2} mol^{-1}. From eq 3 and the definition of relaxation

time, we have in the Langevin model (Appendix C) $\tau_\phi^L = f/k$. From Figure 4 this time (τ_ϕ^L) is of the order of 0.2 ps, which yields an estimate of the friction constant $f = k\tau_\phi \simeq 0.11$ g cm^2 s^{-1} mol^{-1}. The ratio $f^2/4Ik \simeq 0.74$ is less than unity, indicating that the Tyr-21 ring torsional motions are slightly underdamped (i.e., in the absence of random torques, the ring would relax to its equilibrium orientation by damped oscillations; see Chandrasekhar, 1943).

The friction constant, f, may be related to an angular diffusion constant by use of the Einstein formula, $D = k_B T/f$, where k_B is the Boltzmann constant and T is the absolute temperature (308 K). For the Tyr-21 ring torsional motion, one obtains $D = 2.3 \times 10^{11}$ s^{-1}. This value is several times larger than experimental diffusion constants for the corresponding rotational motion of small aromatic molecules in organic solvents. As examples, D = 5.7×10^{10} s^{-1} for neat benzene, 5.3×10^{10} s^{-1} for neat toluene, and 2×10^{10} s^{-1} for neat nitrobenzene; slightly larger values are obtained with low-viscosity solvents, e.g., 7.9×10^{10} s^{-1} for benzene in isopentane (Bauer et al., 1974; Stark et al., 1977). The differences between some of these solution results and that for Tyr-21 are not large, particularly in view of the uncertainty in our estimate of f. Nevertheless, it does appear that the Tyr-21 ring encounters somewhat less friction in the protein than do similar aromatic rings in typical organic solvents.

It is possible that the smaller friction encountered by the Tyr-21 ring is due to the covalent structure of the residues in the cage surrounding the ring. This could prevent the cage atoms from interlocking with the ring as effectively as would free solvent molecules. Comparing Tyr-21 and a typical molecule in liquid benzene, it appears that there is not a great difference in the mean density of neighbor atoms around the aromatic rings. In liquid benzene, the average number of carbon atoms in other molecules which are within 5 Å of a carbon atom in any given molecule is about 15 (Lowden & Chandler, 1975; Narten, 1977). The average number of heavy atoms within 5 Å of a Tyr-21 ring carbon, excluding atoms directly bonded to the ring, is about 16 in the X-ray structure. Thus, if packing differences were to account for the lower friction encountered by the Tyr-21 ring, this would have to be due to differences in the detailed configuration of the ring neighbors, e.g., that there are fewer cage atoms in positions which allow them to randomize the torsional angular velocity of the Tyr-21 ring. This is in accord with the small number of atoms contributing to $E_R(\Delta\phi)$ in the various geometries examined (see Table I). Further, it is shown in the next section that the structure of the surrounding cage in a collisional model for the torsional dynamics of Tyr-21 leads to an estimated friction constant comparable to the one found here.

Additional evidence that the magnitudes of f and D given above are approximately correct and that the frictional effects measured by f derive largely from the nonbonded interactions of the ring with the surrounding cage is found by comparing the above results with two other molecular dynamics calculations. The first of these is a previous simulation of the dynamics of the BPTI molecule with some differences in the energy parameters (McCammon et al., 1977). In this simulation somewhat different values of the bond, bond angles, and dihedral angle force constants than those given in Appendix A were used. Despite these differences, the magnitudes of the atomic position fluctuations and the variation in these fluctuations along the polypeptide chain are very similar in the two simulations (except for differences in the C-terminal ends of the chain; see Appendix B). The atomic position fluctuations are evidently fairly insensitive to variations in the parameters which have been modified. These fluctuations appear to be dominated by nonbonded interactions, providing that the bonds and bond angles are kept reasonably stiff and the dihedral angles are kept reasonably flexible. Variations in the bond and bond angle parameters are primarily reflected in changes in local high-frequency "group" vibrational modes, while variations in the dihedral angle parameters are primarily reflected in modified distributions of small fluctuations (<5°) of the dihedral angles. Of particular significance in the present context is that a somewhat stronger intrinsic potential for twisting the C_{21}^{β}–C_{21}^{γ} dihedral angle (χ_{21}^2) was used in the earlier simulation. The effect of this dihedral angle term was to increase the curvature somewhat at the minimum of the torsional potential of mean force. The resulting force constant was approximately 1.3×10^{12} erg rad^{-2} mol^{-1}, but the decay time for $C_\phi(t)$ was reduced to $\tau_\phi \simeq 0.1$ ps, so that $f \simeq 0.13$ g cm^2 s^{-1} mol^{-1} and $D \simeq 1.9 \times 10^{11}$ s^{-1}; that is, the frictional effects were essentially the same as in the present simulation.

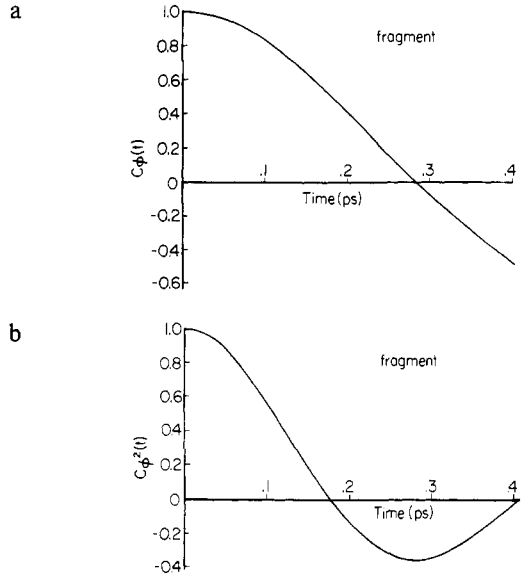

FIGURE 5: (a) The normalized time correlation function for torsional fluctuations of the tyrosine ring in the isolated tyrosine fragment, based on molecular dynamics results. (b) The normalized time correlation function for squared torsional fluctuations of the tyrosine ring in the isolated tyrosine fragment, based on molecular dynamics results.

Comparison can also be made with the results of dynamical simulation of the isolated tyrosine fragment (Figures 5a,b). As noted in the Molecular Dynamics Results section, it is apparent that the tyrosine ring suffers substantially less damping during its torsional motion in the isolated fragment than in intact BPTI. The fact that $C_{\phi^2}(t)$ oscillates about zero suggests that the ring oscillation is "nonergodic" in the fragment simulation; that is, the random torques acting on the ring are sufficiently weak that the torsional oscillations of the ring reflect its initial conditions through most of the simulation (see Appendix E).

Microscopic Models for the Friction

The large size and complicated structure of proteins suggest that it is important to try and find approximate models for representing their dynamic behavior. The simplest such model which has some currency treats the protein as an elastic solid (Suezaki & Gō, 1975). Although this may be of some use for the gross dynamics (e.g., breathing vibrations), it cannot be applied to the phenomena under consideration here. Instead it is necessary to introduce detailed microscopic models of the type that have been developed to account for the dynamics of particles in dense media. Two particularly important examples

are the independent binary collision model (Hynes, 1977), which has been used as a starting point for theories of the dynamics of dense gases and fluids, and the harmonic model, often used as a starting point in theories of the dynamics of solids (Maradudin et al., 1971) and of the internal dynamics of isolated molecules (Wilson et al., 1955). These two models begin with opposite assumptions about the forces associated with typical particle displacements in a medium. In the usual (hard-sphere limit) collisional models, the force on a given particle varies negligibly except during collisions, when the force varies sharply with displacement of the collision partner. In the harmonic model, it is assumed that the temperature, density, and interaction potentials in a system are such that the force on a given particle varies linearly with the typical thermal displacements of other particles in the system.

In this section, we use these two models primarily to exemplify the extreme points of view that may be taken with respect to the microscopic dissipative processes which occur in proteins. We find that either of the models can account for the limited dynamical data available for the tyrosine rings of BPTI. Thus, additional studies will be required to obtain a definitive description of the origin of the observed frictional effects.

Collisional Model. The relaxation of fluctuations of dynamic properties such as the position, orientation, and velocity of particles in gases and liquids has long been a subject of interest in statistical mechanics. One theoretical approach to such problems, pioneered by Enskog (1922) and subsequently developed by Gordon (1966) and Chandler (1974b) among others, pictures the relaxation as occurring as a result of successive binary collisions between the repulsive van der Waals cores of neighboring particles. The successive collisions are assumed to be uncorrelated and instantaneous and to randomize the velocity (or angular velocity) of the struck particles; the particles move freely between collisions. These assumptions are, of course, oversimplified and much of the modern work on simple liquid dynamics is devoted to introducing refinements into the theory. The present consensus (Hynes, 1977) is that the Enskog-type models provide a good first approximation to the microscopic description of dissipation in fluids. Corresponding models have been employed in the study of vibrational relaxation in liquids (Litovitz, 1957; Fischer & Laubereau, 1975). Here, we inquire into the possibility that simple collisional models may be useful in the analysis of internal friction in proteins and, in particular, of frictional effects associated with aromatic ring motions in BPTI. The collisional model used to describe the Tyr-21 ring torsions takes into account that, between collisions, the ring moves in a harmonic manner due to the torsional restoring force. In this regard the model is different from the models used in simple fluids; details of this extension of the Enskog kinetic theory to harmonic oscillator relaxation are given in Appendix D.

The theory developed in Appendix D yields expressions for the time correlation functions $C_\phi(t)$, $C_{\phi^2}(t)$, and $C_\phi(t)$, which depend only on ω_0, the frequency of the oscillator, and τ, the average time between collisions of the oscillator with neighboring particles. The theory predicts that the decay time for $C_\phi(t)$ is $\tau_\phi = (\tau\omega_0^2)^{-1}$ and that the decay time for $C_{\phi^2}(t)$ is $\tau_{\phi^2} = (\tau_\phi/2) + \tau$. If many collisions occur during the period of the unperturbed oscillator one obtains the small-step diffusion limit; in this limit ϕ evolves in accord with the Langevin equation and $\tau_{\phi^2} = \tau_\phi/2$, as expected.

As an estimate for ω_0 for the Tyr-21 ring torsional oscillations, we use the value obtained in the Phenomenological Analysis of Ring Motion section, $\omega_0 = (k/I)^{1/2} \approx 8.6 \times 10^{12}$ s^{-1}. The mean time between collisions, τ, is difficult to calculate in a completely satisfactory way. The complicated structure and bonding of the cage atoms make it difficult to estimate the thermal relative velocities of these atoms along trajectories which would lead to effective collisions with the ring. The mean lengths of these trajectories are also hard to determine. With these reservations in mind, we have obtained a value of τ by the following approximate scheme. We note that the rigid-protein torsional potential for Tyr-21 provides some information on how far cage atoms can move relative to the ring. Del Rio & DeLonngi (1976) have described a method for calculating the mean distance of closest approach of colliding soft particles by averaging over the relative kinetic energies of the collision partners. Their method may be applied in the present case to give, for the mean angle of positive or negative torsional excursion of the ring,

$$\overline{\Delta\phi} = \int_0^{\phi_C} \exp(-E_R/RT)\mathrm{d}\phi \qquad (4)$$

Here, $\phi = 0$ corresponds to the minimum of the rigid-protein potential, $E_R(\phi)$, ϕ_C is an arbitrary cutoff value of ϕ beyond which further contributions to the integral are negligible, and R is the gas constant. Using the protein potential corresponding to the X-ray structure (Figure 3), one finds $\overline{\Delta\phi} \simeq 7°$. The lateral displacement of the ring δ- and ϵ-carbon atoms associated with this angular excursion is 0.15 Å; we take this to be the mean relative distance traveled by a cage atom before there is an effective collision with the ring. The root mean square thermal velocity of a cage atom with the typical mass of 15 g/mol is, at 300 K, $v = 7 \times 10^{12}$ Å/s. Thus, treating the ring as a stationary target and making the simplified kinetic theory assumption that about 1/6 of the displacements of a cage atom will be in the direction of the ring, the average time required for a cage atom to move from its mean position and hit the ring is 1.3×10^{-13} s. Analysis of the dominant interactions in the rigid-protein potentials suggests that there are usually two such atoms in positions to collide with the ring in a way which can alter the Tyr-21 torsional angular velocity (see Table I). Hence, a rough estimate of the mean time between effective collisions is $\tau \simeq 7 \times 10^{-14}$ s.

Several comments may help to clarify the approximations made in the above argument. The rigid-protein potential used to estimate $\overline{\Delta\phi}$ will give an underestimate of the distance any one matrix atom must move to strike the ring if many matrix atoms contribute to E_R. Although E_R is in fact dominated by only a few "head-on" contacts (Table I), a number of softer "grazing" or "oblique" contacts also contribute. However, the resulting underestimate of path lengths and increase in the estimated mean time between collisions would be compensated for in part by a fractional increase in the effective number of collision partners if grazing or oblique collisions were included. In principle, the mean free paths of the cage atoms should be determined by examining a representative set of instantaneous configurations from the simulation and averaging. This lengthy calculation has been avoided in the above argument by taking the X-ray structure as a typical configuration; the approximations inherent in the simple collision theory model do not warrant more detailed analysis. The treatment of the ring as a stationary target can be justified by reference to Figure 4, from which it is apparent that, on average, the ring moves very little in a time $\tau \simeq 7 \times 10^{-14}$ s.

In Figure 6a we compare $C_\phi(t)$ obtained from the simulation with the collisional model result calculated using the parameters estimated from the equilibrium properties of the

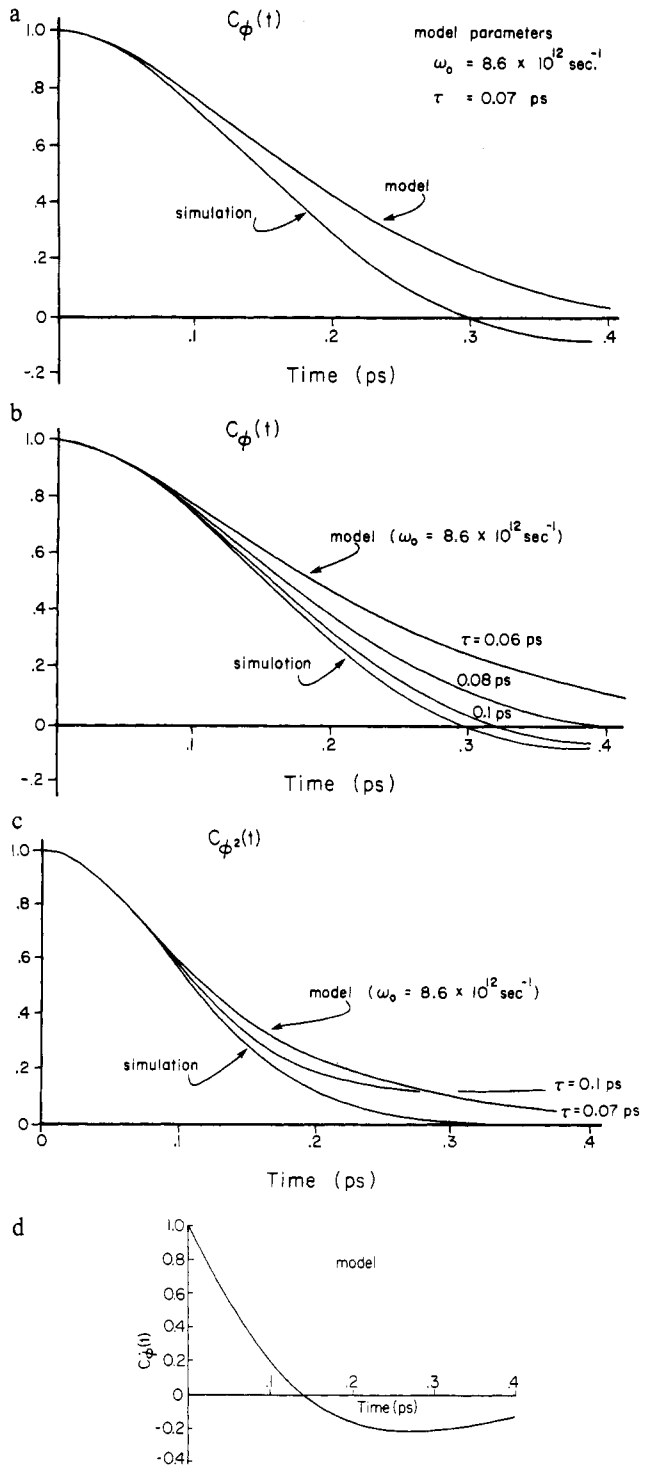

FIGURE 6: (a) Comparison of simulation and collisional model results for the normalized time correlation function for torsional fluctuations of the Tyr-21 ring. (See text for discussion.) (b) Variation in collisional model results for the normalized time correlation function for torsional fluctuations of the Tyr-21 ring upon small adjustments of the parameter τ. (See text for discussion.) (c) Comparison of simulation and collisional model results for the normalized time correlation function for squared torsional fluctuations of the Tyr-21 ring. (See text for discussion.) (d) The normalized time correlation function for the torsional angular velocity of the Tyr-21 ring, based on the collisional model. (See text for discussion; τ = 0.1 ps, ω_0 = 8.6 × 10^{12} s^{-1}.)

protein (i.e., $\omega_0 = 8.6 \times 10^{12}$ s^{-1}, $\tau = 7 \times 10^{-14}$ s). The agreement of the two curves is seen to be good. The uncertainty in our estimate of τ (see above) motivated a study of the variation of the model $C_\phi(t)$ as a function of small changes in τ. The curves presented in Figure 6b illustrate the sensitivity of the model for $C_\phi(t)$ to variations in τ and show that a small increase from the a priori estimate (i.e., to $\tau = 1 \times 10^{-13}$ s) yields excellent agreement with the simulation result. Small variations in ω_0 change the initial curvature of $C_\phi(t)$ and result in poorer agreement with the simulation result.

In Figure 6c we compare the simulation result for $C_{\phi^2}(t)$ with the collisional model results calculated using the a priori ($\omega_0 = 8.6 \times 10^{12}$ s^{-1}, $\tau = 7 \times 10^{-14}$ s) and adjusted ($\omega_0 = 8.6 \times 10^{12}$ s^{-1}, $\tau = 1 \times 10^{-13}$ s) parameters. Again, the a priori model result is in fairly good agreement with the simulation over the interval for which the latter is quantitatively reliable ($t < 0.2$ ps); for this time interval, the model with the adjusted parameters is in excellent agreement with the simulation result. In Figure 6d we show the ring torsional angular velocity time correlation function, $C_{\dot\phi}(t)$, calculated from the collisional model using the adjusted parameters ($\omega_0 = 8.6 \times 10^{12}$ s^{-1}, $\tau = 1 \times 10^{-13}$ s). The cusp at $t = 0$ in the model curve for $C_{\dot\phi}(t)$ is a consequence of assuming that collisions are instantaneous events (Chandler, 1974b). A similar cusp appears in Langevin model curves for $C_{\dot\phi}(t)$ in consequence of the assumption that the random torque term $N_r(t)$ varies infinitely rapidly. At times longer than 0.2 ps the agreement between the simulation and model curves is relatively poor. This would be expected even if the simulation data were known to be correct, since the assumptions of independent binary collision models break down for times greater than 0.1–0.2 ps; at these longer times, correlation effects such as collective cage atom displacements (or hydrodynamic circulation in fluids) become important.

The dynamical predictions of the collisional model described above are very similar but not identical to the predictions of the Langevin model for the harmonic oscillator (see Appendices C and D). The two models give the same expression for $C_\phi(t)$ and $C_{\dot\phi}(t)$ if one makes the identifications $\omega_0^2 = k/I$ and $\tau^{-1} = f/I$. The expressions for $C_{\phi^2}(t)$ differ slightly because, unlike the Langevin model, the velocity fluctuations are not Gaussian in a collisional model. Using the above identifications, however, one may say that the criterion for underdamped motion in the collisional model is $4\omega_0^2 > \tau^{-2}$ or, in terms of decay times, $\tau_{\phi^2}/\tau_\phi > 3/4$. The latter ratio is equal to 0.9 in the collisional model results for Tyr-21.

Harmonic Model. In the harmonic model, it is assumed that the motion of a system of particles is confined to the region of a minimum in the potential energy surface of the system and that the displacements of the particles are small enough that the potential energy can be approximated by the truncated Taylor series

$$V(\{x_i\}) = V(\{x_i^0\}) + \sum_{i,j} f_{ij} \Delta x_i \Delta x_j \qquad (5)$$

where the $\{x_i^0\}$ are the minimum energy coordinates of the particles, $\Delta x_i = x_i - x_i^0$, and the f_{ij} are quadratic force constants. In principle, the harmonic equations of motion may be solved to yield a set of normal modes $\{Q_i(t)\}$ which have a simple oscillatory time dependence and which are linearly related to the $\{\Delta x_i(t)\}$ (Wilson et al., 1955). We have not attempted to solve for the normal modes of BPTI, since the large number of atoms in the molecule makes such a calculation difficult. However, the following formal results for a harmonic system can be used in the analysis of the ring torsion correlation functions. In the small vibration limit, the torsional fluctuations of an aromatic ring can be expressed as a linear combination of the normal coordinates

$$\Delta\phi(t) = \sum a_i Q_i(t) \qquad (6)$$

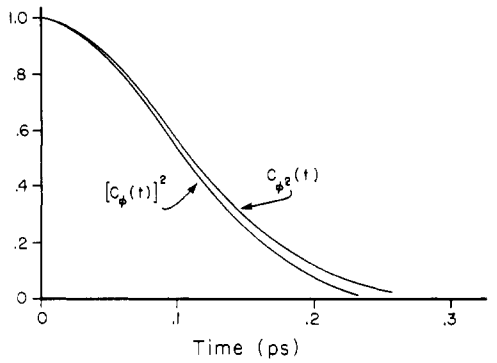

FIGURE 7: Comparison of the simulation results for the normalized time correlation function for the torsional and squared torsional fluctuations.

If this expression is valid, the correlation functions $C_\phi(t) = \langle \Delta\phi(t)\Delta\phi(0)\rangle / \langle [\Delta\phi(0)]^2\rangle$ and $C_{\phi^2}(t) = \langle \Delta\phi^2(t)\Delta\phi^2(0)\rangle / \langle [\Delta\phi^2(0)]^2\rangle$ are related by (see Appendix E)

$$C_{\phi^2}(t) = [C_\phi(t)]^2 \tag{7}$$

The broken brackets in the definitions of $C_\phi(t)$ and $C_{\phi^2}(t)$ indicate ensemble averages; the above relation will not hold for time-averaged correlation functions unless the system is ergodic (see Appendix E).

Over the time interval for which the data are quantitatively reliable ($t \leq 0.2$ ps), the molecular dynamics correlation functions shown in Figures 4a,b obey the above relation (Figure 7). Thus, it cannot be ruled out that the motion in BPTI is largely harmonic and that the diffusional torsional motion of the Tyr-21 ring results from a superposition of independent normal modes.

Discussion

To predict the probability of structural fluctuations in a protein, it is necessary to know the effective conformational energy surface of the molecule. To predict the average dynamical character of such fluctuations, it is necessary to know in addition the frictional effects associated with the various internal motions. It has been demonstrated in this paper, which uses the oscillations of a buried tyrosine ring in BPTI as a model, that a molecular dynamics calculation based on empirical energy functions can provide both the magnitude and time dependence of structural fluctuations. For the tyrosine rings which are in the interior of the protein, it is found that torsional fluctuations on the order of ±30° occur on the picosecond time scale. Further, it was shown by using somewhat different empirical potentials that the character of the dynamics is not very sensitive to the exact parameter values. The frictional effects associated with these motions are sizable, though apparently somewhat smaller than those encountered by aromatic rings undergoing similar motions in organic solvents. As a first approximation the ring torsional dynamics can be quantitatively described in terms of the simple Langevin equation for a harmonic oscillator.

Unfortunately, the present molecular dynamics results are not sufficiently accurate to allow us to discriminate among detailed microscopic models for the frictional processes. It is possible that much longer molecular dynamics simulations of BPTI would yield correlation functions which would be sufficiently accurate to guide the development of such microscopic models. As mentioned before, the difficulty of performing a full normal mode analysis on BPTI hinders the straightforward calculation of correlation functions in the harmonic model. Moment methods could provide a more tractable route for the calculation of harmonic model correlation functions, at least for short times (Platz & Gordon, 1973). The two limiting models presented here define some of the conceptual possibilities for elementary mechanisms of dissipation. It seems possible, for example, that short-time relaxation processes in some interior regions of the protein (e.g., hydrogen-bonded secondary structural elements) are dominated by the interference of harmonic modes, while collisional effects dominate in other regions (e.g., more hydrophobic domains). These suppositions are based on the recognition that the more rigidly bonded regions have interactions which tend to remain harmonic over a wide energy range (bonds, bond angles, and hydrogen bonds) and on the observation that the harmonic approximation breaks down significantly for rare gas (van der Waals) crystals at absolute temperatures above half their melting points (Dickey & Paskin, 1969; Hansen & Klein, 1976). Either model would probably have to be generalized to provide a quantitative description of relaxation at times greater than a few tenths of a picosecond; anharmonic terms could be added in the harmonic model, and the finite duration of collisions could be considered in collisional models. At longer times, structural and dielectric relaxation processes may have to be accounted for. At the surface of a protein molecule in solution, collisional and hydrodynamic coupling to the solvent will be important sources of dissipation (McCammon et al., 1976; McCammon & Wolynes, 1977).

Ultimately, a complete picture of the physical processes which give rise to frictional effects in proteins should help us to understand many important features of these molecules, including the evolution of conditions favorable for the catalytic act in enzymes, the disposition of kinetic energy evolved in elementary reaction steps, and the rates of allosteric transitions. As a simple illustration of this notion, we sketch how frictional effects can influence one particular "reaction" in BPTI: the crossing of a torsional barrier by the Tyr-21 ring. It is known that for sufficiently large frictional effects, the usual transition-state theory rate expression for crossing a smooth potential barrier must be multiplied by a factor which is inversely proportional to the friction constant (Kramers, 1940; Chandrasekhar, 1943). One can picture this frictional effect on the barrier crossing process in a simple way. In transition-state theory, one imagines that each successful trajectory is characterized by direct passage over the barrier. In the large friction case, however, the ring often suffers several collisions with the protein matrix while crossing the barrier and the barrier crossing has a diffusional character. Quantitatively, frictional effects are important when $f/I \gtrsim \omega_B$, where f and I are the friction constant and moment of inertia of the ring (cf. the Phenomenological Analysis of Ring Motion section) and ω_B is the natural frequency associated with the inverted quadratic barrier. If we *assume* that the friction constant, f, is the same for motion over the barrier as for motion near the torsional energy minimum and that the inverted barrier has a similar shape to this minimum, then $\tau^{-1} = f/I \simeq 1.5 \times 10^{13}$ $s^{-1} \gtrsim \omega_B \simeq 8.6 \times 10^{12}$ s^{-1}; the motion of the ring near the top of the barrier is predicted to be influenced by frictional effects, with the crossing rate reduced by the factor $\omega_B\tau \simeq 0.6$. Larger friction coefficients or flatter barriers would lead to greater reduction of the crossing rate and longer residence times in the transition state. It is evident that the consideration of such effects is important in understanding the catalytic mechanisms of enzymes.

Acknowledgments

We thank Bruce Gelin and Peter Rossky for discussions and

for computer programs which have been helpful in this work. We thank John Deutch and Ron Levy for helpful comments and John Ramsdell for valuable assistance with the computer programming and, particularly, the development of the graphics program used for Figure 1.

Appendix

A. *Empirical Energy Function*

The conformational energy of BPTI has been calculated using empirical energy functions. The functional forms chosen for the various types of interactions are outlined below (Gelin & Karplus, 1975).

The energy is composed of terms representing bonds, bond angles, torsional angles, van der Waals interactions, electrostatic interactions, and hydrogen bonds. The resulting expression has the form

$$E(\mathbf{R}) = \frac{1}{2}\sum_{\text{bonds}} K_b(b - b_0)^2 + \frac{1}{2}\sum_{\substack{\text{bond}\\ \text{angles}}} K_\theta(\theta - \theta_0)^2 + \frac{1}{2}\sum_{\substack{\text{torsional}\\ \text{angles}}} K_\phi[1 + \cos(n\phi - \delta)] + \sum_{\substack{\text{nb pairs}\\ r<8\text{Å}}}\left[\frac{A}{r^{12}} - \frac{C}{r^6} + \frac{q_1q_2}{Dr}\right] + \sum_{\text{H bonds}}\left[\frac{A'}{r^{12}} - \frac{C'}{r^{10}}\right] \quad \text{(A1)}$$

The energy is a function of the Cartesian coordinate set, **R**, specifying the positions of all the atoms involved, but the calculation is carried out by first evaluating the internal coordinates for bonds (b), bond angles (θ), dihedral angles (ϕ), and interparticle distances (r) for any given geometry, **R**, and using them to evaluate the contributions to eq A1, which depends on the energy parameters K_b, K_θ, K_ϕ, Lennard-Jones parameters A and C, atomic charges q_i, dielectric constants D, hydrogen-bond parameters A' and C', and geometrical reference values ("zero values") b_0, θ_0, n, and δ. As in previous work, the protein is represented by extended atoms; one extended atom replaces a nonhydrogen atom and any hydrogens bonded to it. Table AI gives the extended atom set used in this work, along with the van der Waals parameters. Table AII gives the rest of the parameters used for the calculations, except for the atom charges, which are given in Table AIII. In the Lennard-Jones potential function, $Ar^{-12} - Cr^{-6}$, the parameter C is determined from the Slater–Kirkwood formula (Slater & Kirkwood, 1939), and A is calculated from $A = {}^1/_2C(r_i + r_j)^6$, where r_i and r_j are the van der Waals radii for the pair of atoms under consideration. Four solvent molecules which are internally bound are included in the list of protein atoms. Solvent molecules are represented as extended atoms which interact by van der Waals and hydrogen-bond forces with protein atoms (the solvent atoms are electrically neutral). The dielectric constant has been taken as $D(r) = r$. This choice makes a computationally convenient expression for nonbonded energies, as only even powers of r are required; also, it is numerically valid in the regions of the most important interactions (from 2 to 5 Å where D varies from 2 to 5). A fixed list of nonbonded atom pairs was used throughout the molecular dynamics calculation. This list included all pairs which are separated by three or more bonds and which have nonbonded distances less than 8 Å in the X-ray structure. The large cutoff distance was chosen to allow for pairs which may move into ranges of significant nonbonded interaction during the course of the simulation. A fixed list of hydrogen-bonded pairs was also used throughout the simulation; these pairs, which are listed in Table AIV, were ones which are appropriately positioned for hydrogen bonding in the X-ray structure.

Table AI: Extended Atoms and Their Nonbonded Parameters

atom symbol	α[a]	N_{eff}[b]	r_{vdW}[c]	groups represented
O	0.84	6	1.60	carbonyl oxygen
OH	1.20	7	1.70	alcoholic hydroxyl (Ser, Thr, Tyr); H_2O
OM	2.14	6	1.60	carboxyl oxygen (Asp, Glu, carboxy terminus)
NH	1.40	7	1.65	peptide nitrogen, whether -N- or -NH; other -NH- groups
N(2)	1.70	8	1.70	$-NH_2$ terminals (Asn, Gln, Arg)
N(3)	2.13	9	1.75	$-NH_3^+$ terminals (Lys, amino terminal)
CH	1.35	6	1.85	aliphatic -CH group
C(2)	1.77	7	1.90	aliphatic $-CH_2$ group
C(3)	2.17	8	1.95	methyl terminal $-CH_3$
C	1.65	5	1.80	aromatic or carbonyl carbon
CR	2.07	6	1.90	aromatic -CH group
S	0.34	16	1.90	sulfur (Cys, Met)

[a] Polarizability (Å^3). [b] "Effective" outer-shell electron number. [c] van der Waals radius (Å).

B. *Molecular Dynamics Calculation*

As in the previously reported simulation (McCammon et al., 1977), the dynamics of the 454 heavy atoms of BPTI and of the four internal water molecules were calculated by numerically integrating the classical equations of motion for these atoms. No constraints were introduced to simplify the system and all of the atoms were allowed to move in accord with the potential function described in Appendix A. The integration was performed by means of the fifth-order Gear algorithm (Gear, 1966, 1971). In this scheme, the atomic positions and their time derivatives at time $t + \Delta t$ are predicted from the corresponding quantities at time t by means of Taylor series

$$\begin{aligned} X_0' &= X_0 + X_1 + X_2 + X_3 + X_4 + X_5 \\ X_1' &= X_1 + 2X_2 + 3X_3 + 4X_4 + 5X_5 \\ X_2' &= X_2 + 3X_3 + 6X_4 + 10X_5 \\ X_3' &= X_3 + 4X_4 + 10X_5 \\ X_4' &= X_4 + 5X_5 \end{aligned} \quad \text{(B1)}$$

where $X_n = [(\Delta t)^n n!]\, d^n x/dt^n$, the unprimed quantities correspond to time t, the primed quantities correspond to time $t + \Delta t$, and X represents a Cartesian position component of any one of the 458 atoms. The forces acting on the atoms in the predicted configuration are computed from the potential energy function, and these forces are used to correct the predicted atomic positions and time derivatives by the equations

$$\begin{aligned} X_0(t + \Delta t) &= X_0' + (3/16)A \\ X_1(t + \Delta t) &= X_1' + (251/360)A \\ X_2(t + \Delta t) &= X_2' + (1)A \\ X_3(t + \Delta t) &= X_3' + (11/18)A \\ X_4(t + \Delta t) &= X_4' + (1/6)A \\ X_5(t + \Delta t) &= X_5' + (1/60)A \end{aligned} \quad \text{(B2)}$$

where $A = [(\Delta t)^2/2]f' - X_2'$, and f' is the force component corresponding to X in the predicted configuration. A time step of $\Delta t = 9.78 \times 10^{-16}$ s was found to yield accurate results over the time period of the simulation.

The results described here were obtained after a more

Table AII: Parameters for Bonded, Bond-Angle, Torsional, and Hydrogen-Bonded Interactions

Bond Energy Function, $^1/_2K_b(b - b_0)^2$

bond type	$^1/_2K_b$ [kcal/(mol A^2)]	b_0 (A)
CH-OH	400	1.420
CH-NH	450	1.461
CH-N(3)	450	1.469
CH-CH	400	1.531
C(2)-OH	400	1.420
C(2)-NH	450	1.458
C(2)-N(3)	450	1.479
C(2)-CH	400	1.523
C(2)-C(2)	400	1.518
C(3)-CH	400	1.518
C(3)-C(2)	400	1.541
C-O	600	1.234
C-OH	450	1.378
C-OM	450	1.222
C-NH	500	1.317
C-N(2)	450	1.333
C-CH	400	1.517
C-C(2)	400	1.517
CR-C	500	1.352
CR-CR	500	1.388
S-C(2)	450	1.814
S-C(3)	450	1.769
S-S	500	2.015

Torsional Energy Function, $^1/_2K_\phi[1 + \cos(n\phi - \delta)]$

torsion type	$^1/_2K_\phi$ (kcal/mol)	n (dimensionless)	δ (deg)
X-CH-NH-Y	0.3	3	180
X-CH-CH-Y	0.5	3	0
X-C(2)-NH-Y	0.3	3	180
X-C(2)-CH-Y	0.5	3	0
X-C(2)-C(2)-Y	0.5	3	0
X-C-NH-Y	7.0	2	180
X-C-CH-Y	0.1	3	0
X-C-C(2)-Y	0.1	3	0
X-CR-C-Y	10.0	2	180
X-CR-CR-Y	10.0	2	180
X-S-C(2)-Y	0.5	2	0
X-S-S-Y	4.0	2	0

Hydrogen Bond Function, $A'r^{-12} - C'r^{-10}$

bond type	E_{min} (kcal/mol) $= -0.067\ C'^6/A'^5$	R_{min} (A) $= (1.2\,A'/C')^{1/2}$
OH···O	−3.5	2.80
OH···OH	−3.5	2.75
OH···OM	−3.5	2.85
NH···O	−3.0	2.95
NH···OH	−3.0	3.08
NH···OM	−3.0	3.10
N(2)···O	−2.5	2.87
N(2)···OH	−2.5	2.87
N(2)···OM	−2.5	2.87
N(3)···OH	−2.5	3.00

Bond Angle Energy Function, $^1/_2K_\theta(\theta - \theta_0)^2$

angle type	$^1/_2K_\theta$ [kcal/(mol rad^2)]	θ_0 (deg)
OM-C-OM	50	129.0
NH-C-O	60	124.5
N(2)-C-O	60	120.6
N(2)-C-NH	60	117.0
N(2)-C-N(2)	60	120.3
CH-C-O	50	122.3
CH-CH-OH	50	101.5
CH-C(2)-OH	50	109.3
CH-C-OM	40	118.0
CH-CH-NH	50	107.1
CH-C-NH	35	117.5
CH-C(2)-CH	30	113.2
C(2)-C-O	50	123.5
C(2)-C-OM	40	115.9
C(2)-CH-NH	30	109.0
C(2)-C(2)-NH	50	109.6
C(2)-C-NH	35	115.0
C(2)-C-N(2)	50	116.0
C(2)-CH-N(3)	50	108.9
C(2)-C(2)-N(3)	30	109.8
C(2)-NH-CH	70	117.4
C(2)-CH-CH	30	108.9
C(2)-C(2)-CH	30	111.8
C(2)-C(2)-C(2)	30	109.5
C(3)-CH-OH	30	110.5
C(3)-CH-NH	30	108.6
C(3)-CH-CH	50	107.8
C(3)-C(2)-CH	30	108.8
C(3)-CH-C(2)	30	108.9
C(3)-S-C(2)	50	97.2
C(3)-CH-C(3)	30	110.7
C-CH-NH	60	108.6
C-C(2)-NH	90	110.5
C-CH-N(3)	50	118.3
C-NH-CH	60	119.1
C-CH-CH	30	107.5
C-C(2)-CH	50	110.4
C-NH-C(2)	60	117.8
C-CH-C(2)	30	107.1
C-C(2)-C(2)	30	110.4
C-CH-C(3)	50	104.3
CR-C-OH	50	118.3
CR-C-C(2)	50	122.6
CR-CR-C	50	121.3
CR-CR-CR	50	123.5
S-C(2)-CH	50	117.2
S-C(2)-C(2)	50	110.2
S-S-C(2)	50	104.2

careful equilibration of the system prior to data collection than was used in the previous work. The present simulation was initiated by assigning all atoms in the X-ray structure velocities with equal magnitudes (corresponding to 300 K) and randomized directions. The initial accelerations were computed from the forces acting on the atoms in the X-ray structure; all higher derivatives were initially set to zero. During the first 2.0 ps of the trajectory calculation, the atomic velocities were modified as necessary to maintain the protein temperature at about 300 K and to prevent localized heating due to the nonuniform stresses in the X-ray structure. The overall temperature was maintained by multiplying all atomic velocities by 1.005 or 0.995 after any step in which the average BPTI temperature was less than 295 K or greater than 305 K, respectively. Localized heating was prevented by multiplying the velocity of an atom by a factor slightly less than unity after any step in which that atom's temperature exceeded 670 K. This special treatment of certain atoms imparted a small net linear and angular velocity to the protein; the resulting overall motion was stopped after the first 2.0 ps. The equilibration period was continued for an additional 2.9 ps without any external modifications of the atomic velocities to allow more complete relaxation of the protein. The average temperature attained during this period was 308 K. The final phase of the simulation (9.8 ps) provided the trajectory used for statistical analysis; the average temperature during this period was again 308 K. The time required to compute the entire 14.7-ps trajectory was slightly more than 2 h on an IBM 360/91 computer.

As a result of the careful equilibration used in the present

Table AIII: Atom Charges

residue[a]	N	C^{α}	C′	O	side chain atoms				
Ala	−0.080	0.075	0.350	−0.365	C^{β} (0.020)				
Arg[b]	−0.080	0.075	0.352	−0.365	C^{β} (0.039)	C^{γ} (0.044)	C^{δ} (0.115)	N^{ϵ} (−0.029)	C^{ζ} (0.460)
					$N^{\eta 1}$ (0.192)	$N^{\eta 2}$ (0.192)			
Asn	−0.075	0.092	0.350	−0.357	C^{β} (−0.015)	C^{γ} (0.355)	$O^{\delta 1}$ (−0.365)	$N^{\delta 2}$ (0.015)	
Asp[b]	−0.110	0.070	0.355	−0.380	C^{β} (−0.150)	C^{γ} (0.365)	$O^{\delta 1}$ (−0.575)	$O^{\delta 2}$ (−0.575)	
Cys[c]	−0.075	0.092	0.350	−0.357	C^{β} (0.040)	S^{γ} (−0.050)			
Gln	−0.080	0.065	0.350	−0.362	C^{β} (0.042)	C^{γ} (−0.016)	C^{δ} (0.361)	$O^{\epsilon 1}$ (−0.370)	$N^{\epsilon 2}$ (0.010)
Glu[b]	−0.095	0.050	0.355	−0.380	C^{β}(0.010)	C^{γ} (−0.155)	C^{δ} (0.365)	$O^{\epsilon 1}$ (−0.575)	$O^{\epsilon 2}$ (−0.575)
Gly	−0.080	0.090	0.345	−0.355					
His[d]	−0.080	0.075	0.348	−0.360	C^{β} (0.010)	C^{γ} (0.050)	$N^{\delta 1}$ (0.017)	$C^{\delta 2}$ (−0.015)	$C^{\epsilon 1}$ (0.145)
					$N^{\epsilon 2}$ (−0.190)				
Ile	−0.080	0.075	0.350	−0.365	C^{β} (0.028)	$C^{\gamma 1}$ (0.012)	$C^{\gamma 2}$ (−0.012)	$C^{\delta 2}$ (−0.008)	
Leu	−0.080	0.075	0.350	−0.365	C^{β} (0.018)	C^{γ} (0.030)	$C^{\delta 1}$ (−0.014)	$C^{\delta 2}$ (−0.014)	
Lys[b]	−0.090	0.080	0.348	−0.360	C^{β} (0.040)	C^{γ} (0.054)	C^{δ} (0.063)	C^{ϵ} (0.205)	N^{ζ} (0.660)
Met	−0.080	0.075	0.350	−0.365	C^{β} (0.040)	C^{γ} (0.004)	S^{δ} (−0.170)	C^{ϵ} (0.146)	
Phe	−0.080	0.075	0.350	−0.365	C^{β} (0.005)	C^{γ} (0.039)	$C^{\delta 1}$ (−0.019)	$C^{\delta 2}$ (−0.019)	$C^{\epsilon 1}$ (0.010)
					$C^{\epsilon 2}$ (0.010)	C^{ζ} (−0.006)			
Pro	−0.176	0.075	0.350	−0.365	C^{β} (0.029)	C^{γ} (0.008)	C^{δ} (0.079)		
Ser	−0.080	0.060	0.360	−0.363	C^{β} (0.130)	O^{γ} (−0.107)			
Thr	−0.080	0.060	0.360	−0.363	C^{β} (0.140)	$O^{\gamma 1}$ (−0.130)	$C^{\gamma 2}$ (0.013)		
Trp	−0.080	0.075	0.350	−0.365	C^{β} (0.010)	C^{γ} (−0.018)	$C^{\delta 1}$ (0.021)	$C^{\delta 2}$ (−0.023)	$N^{\epsilon 1}$ (−0.016)
					$C^{\epsilon 2}$ (0.140)	$C^{\epsilon 3}$ (−0.003)	$C^{\zeta 2}$(−0.072)	$C^{\zeta 3}$(−0.035)	$C^{\eta 2}$ (0.016)
Tyr	−0.085	0.075	0.352	−0.368	C^{β} (0.006)	C^{γ} (0.024)	$C^{\delta 1}$ (0.002)	$C^{\delta 2}$(0.002)	$C^{\epsilon 1}$ (−0.025)
					$C^{\epsilon 2}$ (−0.025)	C^{ζ} (0.162)	O^{η} (−0.120)		
Val	−0.080	0.075	0.350	−0.365	C^{β} (0.062)	$C^{\gamma 1}$(−0.021)	$C^{\gamma 2}$(−0.021)		

[a] For the amino-terminal residue the charge on N is increased by 0.71 and on C^{α} by 0.02. For the carboxy terminal the charge on C′ is increased by 0.03, on O by −0.20, and a second carboxyl oxygen is introduced, with charge of −0.560. [b] Arg and Lys are assumed to be protonated (net charge +1); Asp and Glu are assumed to be ionized (net charge −1). [c] If a disulfide bridge is formed, both C^{β} charges are reduced by 0.018 and both S^{γ} charges are increased by 0.018. [d] His is treated as having $N^{\delta 1}$ protonated but not $N^{\epsilon 2}$.

calculation, the mean atomic kinetic energies are quite uniform throughout the protein. In particular, the mean kinetic energies of the atoms at the C-terminal end of the polypeptide chain are similar to those in the rest of the protein. In the previously reported simulation, the C-terminal end was significantly warmer than the rest of the protein as a result of sizable local stresses in this model-built part of the X-ray structure (McCammon et al., 1977). Thus, the root mean square fluctuation of C_{58}^{α} about its mean position in the present simulation is somewhat smaller than that found previously (1.3 vs. 2.2 Å). The root mean square fluctuations of most other α carbons are the same to within 0.2 Å in the two simulations.

C. Langevin Equation for an Oscillator

In this appendix we present some results for the correlation functions corresponding to the Langevin equation (I is the moment of inertia, k is the harmonic force constant, and f is the friction constant)

$$I\ddot{\phi} + f\dot{\phi} + k\phi = N_r(t) \qquad \text{(C1)}$$

Multiplying eq C1 by $\phi(0)$, averaging and dividing through by $\langle[\phi(0)]^2\rangle$ yields an equation for the normalized time correlation function, $C_{\phi}^{L}(t)$, in the Langevin model

$$I\ddot{C}_{\phi}^{L} + f\dot{C}_{\phi}^{L} + kC_{\phi}^{L} = 0 \qquad \text{(C2)}$$

where we have used the fact that $\langle\phi(0)N_r(t)\rangle = 0$; the broken brackets, $\langle\ \rangle$, indicate an ensemble average. With known equal-time correlation functions [$C_{\phi}^{L}(0) = 1$, $\dot{C}_{\phi}^{L}(0) = 0$] as initial conditions, eq C2 yields the solution

$$C_{\phi}^{L}(t) = e^{-\beta t/2}[\cos at + (\beta/2a)\sin at] \qquad \text{(C3)}$$

where $a^2 = \omega_0^2 - (\beta^2/4)$, $\omega_0^2 = k/I$, and $\beta = f/I$. The Laplace transform of eq C3 is

$$\hat{C}_{\phi}^{L}(s) = \frac{s + \beta}{s^2 + \beta s + \omega_0^2} \qquad \text{(C4)}$$

Table AIV: Hydrogen-Bonded Pairs[a]

1	$N_1^{\epsilon}\cdots O_{55}$	24	$N_{50}\cdots O_{47}^{\gamma}$
2	$N_5\cdots O_2$	25	$N_{51}\cdots O_{47}$
3	$N_6\cdots O_3$	26	$N_{52}\cdots O_{48}$
4	$O_{11}^{\gamma 1}\cdots O_{34}$	27	$N_{53}\cdots O_{49}$
5	$N_{16}\cdots O_{36}$	28	$N_{53}^{\eta 2}\cdots O_{50}^{\delta 1}$
6	$N_{18}\cdots O_{35}$	29	$N_{54}\cdots O_{50}$
7	$N_{20}\cdots O_{33}$	30	$O_{54}^{\gamma 1}\cdots O_{50}$
8	$N_{20}^{\eta 1}\cdots O_{44}^{\delta 1}$	31	$N_{55}\cdots O_{51}$
9	$N_{21}\cdots O_{45}$	32	$N_{56}\cdots O_{52}$
10	$N_{22}\cdots O_{31}^{\delta 1}$	33	$W1\cdots O_7^{\epsilon 2}$
11	$N_{23}\cdots O_{43}$	34	$W1\cdots O_8$
12	$N_{24}\cdots O_{29}$	35	$W2\cdots W1$
13	$N_{24}^{\delta 2}\cdots O_{31}^{\epsilon 1}$	36	$W2\cdots O_{43}$
14	$N_{27}\cdots O_{24}$	37	$N_{10}\cdots W2$
15	$N_{28}\cdots O_{24}$	38	$W4\cdots W2$
16	$N_{31}\cdots O_{22}$	39	$W4\cdots O_{10}$
17	$N_{33}\cdots O_{20}$	40	$N_{41}\cdots W4$
18	$N_{35}\cdots O_{18}$	41	$N_{44}^{\delta 2}\cdots W4$
19	$N_{36}\cdots O_{11}$	42	$W3\cdots O_{11}$
20	$N_{43}\cdots O_7^{\epsilon 2}$	43	$W3\cdots O_{38}$
21	$N_{43}^{\delta 2}\cdots O_7$	44	$N_{14}\cdots W3$
22	$N_{43}^{\delta 2}\cdots O_{23}$	45	$N_{38}\cdots W3$
23	$N_{45}\cdots O_{21}$		

[a] W1, W2, W3, and W4 are the four internal water molecules.

Equations C3 and C4 will be seen to have the same form as the corresponding collisional model results (see Appendix D).

An expression for $C_{\phi^2}^{L}(t)$ can be found in a straightforward manner (see eq D9–13 of Appendix D). It is

$$C_{\phi^2}^{L}(t) = \frac{1}{4a^2}(2\omega_0^2 e^{-\beta t} - r_1^2 e^{2r_2 t} - r_2^2 e^{2r_1 t}) \qquad \text{(C5)}$$

where r_1 and r_2 are given by the simultaneous equations $r_1 r_2 = \omega_0^2$ and $r_1 + r_2 = -\beta$. Laplace transformation of eq C5 yields

$$\hat{C}_{\phi^2}^{L}(s) = \frac{s^2 + 3s\beta + 2\beta^2 + 2\omega_0^2}{s^3 + 3s^2\beta + 2s\beta^2 + 2s\omega_0^2 + 4\beta\omega_0^2} \qquad \text{(C6)}$$

which is somewhat different from the collisional result (see

Appendix D). The relaxation times τ [$\tau_A = \int_0^\infty C_A(t)\,dt$] for displacements and squared displacements of the oscillator in the Langevin model are

$$\tau_\phi{}^L = \hat{C}_\phi{}^L(s = 0) = \beta/\omega_0{}^2 \tag{C7}$$

$$\tau_{\phi^2}{}^L = \hat{C}_{\phi^2}{}^L(s = 0) = \frac{\beta^2 + \omega_0{}^2}{2\omega_0{}^2\beta} \tag{C8}$$

Measurement of these times from the areas under the calculated $C_\phi(t)$ and $C_{\phi^2}(t)$ allows one to estimate the restoring force and damping constants for a system whose moment of inertia is known and which is assumed to obey the simple Langevin equation, eq C1.

D. Collisional Relaxation of an Oscillator

In this appendix, we consider a simplified model which allows one to calculate the effect of collisions on a harmonic oscillator. The equation of motion of the isoiated oscillator (i.e., neglecting collisions) is

$$I\ddot{\phi} + k\phi = 0 \tag{D1}$$

where we have assumed that $\langle\phi\rangle = 0$ and have used notation appropriate for a torsional oscillator (see eq C1).

The unperturbed oscillator exhibits undamped vibrations at a frequency $\omega_0 = \sqrt{k/I}$. The displacement of the oscillator at time t is given in terms of its initial displacement $\phi(0)$ and initial angular momentum $J(0)$ as

$$\phi(t) = \phi(0)\cos\omega_0 t + \frac{J(0)}{I\omega_0}\sin\omega_0 t \tag{D2}$$

The corresponding normalized time correlation function for displacements of the unperturbed oscillator is

$$C_\phi{}^0(t) = \frac{\langle\phi(t)\phi(0)\rangle^0}{\langle[\phi(0)]^2\rangle} \tag{D3}$$

where the broken brackets indicate an ensemble average and the superscript zero indicates the absence of collisions. By multiplying eq D2 by $\phi(0)$ and averaging, it is possible to express the numerator of eq D3 in terms of equal-time correlation functions whose values are known from the properties of the system at thermal equilibrium (Zwanzig, 1965); we find

$$\langle\phi(t)\phi(0)\rangle^0 = \langle[\phi(0)]^2\rangle\cos\omega_0 t + \frac{\langle\phi(0)J(0)\rangle}{I\omega_0}\sin\omega_0 t \tag{D4a}$$

For an equilibrium system

$$\langle\phi(0)J(0)\rangle = \frac{I}{2}\left\langle\frac{d}{dt}[\phi(0)]^2\right\rangle = 0 \tag{D4b}$$

so that eq D3 becomes

$$C_\phi{}^0(t) = \cos\omega_0 t \tag{D5}$$

The Laplace transform of $C_\phi{}^0(t)$ is

$$\hat{C}_\phi{}^0(s) = \int_0^\infty e^{-st}C_\phi{}^0(t)\,dt = \frac{s}{s^2 + \omega_0{}^2} \tag{D6}$$

The normalized time correlation function for squared displacements of the unperturbed oscillator is

$$C_{\phi^2}{}^0(t) = \frac{\langle\Delta\phi^2(t)\Delta\phi^2(0)\rangle^0}{\langle\Delta\phi^2(0)\Delta\phi^2(0)\rangle} \tag{D7}$$

where, e.g., $\Delta\phi^2(t) = [\phi(t)]^2 - \langle[\phi(0)]^2\rangle = \phi^2(t) - \langle\phi^2(0)\rangle$. The denominator can be written as

$$\langle\Delta\phi^2(0)\Delta\phi^2(0)\rangle = \langle\phi^4(0)\rangle - \langle\phi^2(0)\rangle^2 = 2\langle\phi^2(0)\rangle^2 \tag{D8}$$

The second equality in eq D8 follows from the Gaussian character of ϕ; a Gaussian random variable, $G(t)$, with zero mean has the property (Parzen, 1962)

$$\langle G_1G_2G_3G_4\rangle = \langle G_1G_2\rangle\langle G_3G_4\rangle + \langle G_1G_3\rangle\langle G_2G_4\rangle + \langle G_1G_4\rangle\langle G_2G_3\rangle \tag{D9}$$

where $G_1 \equiv G(t_1)$, etc. The numerator of eq D7 can be written as

$$\langle\Delta\phi^2(t)\Delta\phi^2(0)\rangle^0 = \langle\phi^2(t)\phi^2(0)\rangle^0 - \langle\phi^2(0)\rangle^2 \tag{D10}$$

The function $\langle\phi^2(t)\phi^2(0)\rangle^0$ is most easily evaluated by using eq D9 again,

$$\begin{aligned}\langle\phi^2(t)\phi^2(0)\rangle^0 &= \langle\phi^2(0)\rangle^2 + 2(\langle\phi(t)\phi(0)\rangle^0)^2\\ &= \langle\phi^2(0)\rangle^2 + 2\langle\phi^2(0)\rangle^2\cos^2\omega_0 t\\ &= 2\langle\phi^2(0)\rangle^2 + \langle\phi^2(0)\rangle^2\cos 2\omega_0 t\end{aligned} \tag{D11}$$

where in the first equality we have used the equilibrium result $\langle\phi^2(t)\rangle = \langle\phi^2(0)\rangle$. Equation D11 can also be obtained by squaring eq D2 and proceeding as in the derivation of eq D4a. Using eq D11 in eq D10, we obtain

$$\langle\Delta\phi^2(t)\Delta\phi^2(0)\rangle^0 = \langle\phi^2(0)\rangle^2[1 + \cos 2\omega_0 t] \tag{D12}$$

Equations D7, D8, and D12 give the desired correlation function

$$C_{\phi^2}{}^0(t) = \frac{1}{2}(1 + \cos 2\omega_0 t) \tag{D13}$$

The Laplace transform of $C_{\phi^2}{}^0(t)$ is

$$\hat{C}_{\phi^2}{}^0(s) = \frac{1}{2}\left(\frac{1}{s} + \frac{s}{s^2 + 4\omega_0{}^2}\right) \tag{D14}$$

To obtain an approximate description of the effect of collisions with neighboring particles upon the motion of a harmonic oscillator, we make the simplifying assumptions that the collisions are instantaneous and uncorrelated and that each collision randomizes the momentum of the oscillator. Then the Laplace transforms of the time correlation functions for the displacement and squared displacement of the oscillator are given by (Gordon, 1966; Chandler, 1974b)

$$\hat{C}_\phi(s) = \frac{\hat{C}_\phi{}^0(s + \nu)}{1 - \nu\hat{C}_\phi{}^0(s + \nu)} \tag{D15}$$

$$\hat{C}_{\phi^2}(s) = \frac{\hat{C}_{\phi^2}{}^0(s + \nu)}{1 - \nu\hat{C}_{\phi^2}{}^0(s + \nu)} \tag{D16}$$

where $\nu = \tau^{-1}$ is the reciprocal of the mean time between collisions.

Use of eq D6 and D14 in eq D15 and D16, respectively, yields

$$\hat{C}_\phi(s) = \frac{s + \nu}{s^2 + \nu s + \omega_0{}^2} \tag{D17}$$

$$\hat{C}_{\phi^2}(s) = \frac{s^2 + 2s\nu + \nu^2 + 2\omega_0{}^2}{s^3 + 2s^2\nu + s\nu^2 + 4s\omega_0{}^2 + 2\omega_0{}^2\nu} \tag{D18}$$

The relaxation times for displacements and squared displacements of the oscillator are

$$\tau_\phi = \int_0^\infty C_\phi(t)\,dt = \hat{C}_\phi(s=0) = \nu/\omega_0^2 \quad \text{(D19)}$$

$$\tau_{\phi^2} = \int_0^\infty C_{\phi^2}(t)\,dt = \hat{C}_{\phi^2}(s=0) = \frac{\nu^2 + 2\omega_0^2}{2\omega_0^2\nu} \quad \text{(D20)}$$

Inverse Laplace transformation of eq D17 yields an explicit expression for the displacement time correlation function of the oscillator

$$C_\phi(t) = e^{-\nu t/2}\left[\cos at + \left(\frac{\nu}{2a}\right)\sin at\right] \quad \text{(D21)}$$

where $a^2 = \omega_0^2 - (\nu^2/4)$. Comparing eq D21 with eq C3 we see that they have the same form. The time correlation function for the angular velocity of the oscillator can be obtained from this expression by calculating $d^2[C_\phi(t)]/dt^2$ and normalizing the result; we find

$$C_\phi(t) = e^{-\nu t/2}\left[\cos at - \left(\frac{\nu}{2a}\right)\sin at\right] \quad \text{(D22)}$$

E. Harmonic Relaxation

In the harmonic approximation, the torsional fluctuations of an aromatic ring (or any other linear function of the coordinate displacements) can be written as a linear combination of normal modes

$$\Delta\phi(t) = \sum a_i Q_i(t) \quad \text{(E1)}$$

The time correlation function for torsional fluctuations can then be written as (see eq D3–5)

$$\langle\Delta\phi(t)\Delta\phi(0)\rangle = \sum a_i a_j\langle Q_i(t)Q_j(0)\rangle = \sum_{ij} a_i^2\langle Q_i(t)Q_i(0)\rangle = k_B T\sum_i \frac{a_i^2}{k_i}\cos\omega_i t \quad \text{(E2)}$$

where k_i and ω_i are the force constant and angular frequency associated with the normal coordinate $Q_i(t)$; the quantity $\langle[Q_i(0)]^2\rangle = k_B T/k_i$. The next to the last equality follows from the independence of the normal modes. Normalizing the above result, one obtains

$$C_\phi(t) = \frac{\langle\Delta\phi(t)\Delta\phi(0)\rangle}{\langle[\Delta\phi(0)]^2\rangle} = \frac{\sum_i \frac{a_i^2}{k_i}\cos\omega_i t}{\sum_i \frac{a_i^2}{k_i}} \quad \text{(E3)}$$

The time correlation function for the squared torsional fluctuation is

$$\langle\Delta\phi^2(t)\Delta\phi^2(0)\rangle = \langle\phi^2(t)\phi^2(0)\rangle - \langle\phi^2(0)\rangle^2 = \sum_{ijkl} a_i a_j a_k a_l\langle Q_i(t)Q_j(t)Q_k(0)Q_l(0)\rangle - [\sum_{ij} a_i a_j\langle Q_i(0)Q_j(0)\rangle]^2 \quad \text{(E4)}$$

Simplifying this result and normalizing, we obtain the normalized time correlation function for squared torsional fluctuations

$$C_{\phi^2}(t) = \frac{\langle\Delta\phi^2(t)\Delta\phi^2(0)\rangle}{\langle\Delta\phi^2(0)\Delta\phi^2(0)\rangle} = [C_\phi(t)]^2 \quad \text{(E5)}$$

where the last equality follows from the fact that a sum of Gaussian variables is itself Gaussian (Parzen, 1962) and by application of eq D9.

All the averages taken above are ensemble averages, so these relations hold for the time averages of ergodic systems only. This distinction can be important in molecular dynamics calculations on nearly harmonic systems, since the time evolution of such systems has been observed to be nonergodic during dynamical simulations (Dickey & Paskin, 1969). The following results for a single oscillator illustrate the effects of nonergodic behavior. For the oscillator defined by eq D1 with the solution given by eq D2, the *time averaged* correlation functions can be shown to be

$$\langle\phi(t)\phi(0)\rangle_T \equiv \lim_{T\to\infty}\frac{1}{T}\int_0^T ds\;\phi(t+s)\phi(s) = \frac{1}{2}\left[\phi^2(0) + \frac{J^2(0)}{I^2\omega_0^2}\right]\cos\omega_0 t \quad \text{(E6)}$$

or, normalizing,

$$C_\phi^T(t) = \frac{\langle\phi(t)\phi(0)\rangle_T}{\langle\phi(0)\phi(0)\rangle_T} = \cos\omega_0 t \quad \text{(E7)}$$

and

$$\langle\Delta\phi^2(t)\Delta\phi^2(0)\rangle_T \equiv \lim_{T\to\infty}\frac{1}{T}\int_0^\infty ds\;\Delta\phi^2(t+s)\Delta\phi^2(s) = \langle\phi^2(t)\phi^2(0)\rangle_T - \langle\phi^2(0)\rangle_T^2 = \frac{1}{8}\left[\phi^2(0) + \frac{J^2(0)}{I^2\omega_0^2}\right]^2\cos 2\omega_0 t \quad \text{(E8)}$$

or, normalizing,

$$C_{\phi^2}^T(t) = \frac{\langle\Delta\phi^2(t)\Delta\phi^2(0)\rangle_T}{\langle\Delta\phi^2(0)\Delta\phi^2(0)\rangle_T} = \cos 2\omega_0 t \quad \text{(E9)}$$

Note that while eq E7 is identical to eq D5, eq E9 differs from eq D13 and that eq E5 is not satisfied by these time averaged correlation functions. The usual ensemble average result is obtained upon averaging over initial conditions in eq E6, but to obtain the correct squared fluctuation correlation function, one must be careful to subtract $\langle\langle\phi^2(0)\rangle_T\rangle^2$ and not $\langle\langle\phi^2(0)\rangle_T^2\rangle$ in the operation corresponding to the second equality of eq E8. The difference between these two quantities is seen by calculating their values; the results are

$$\langle\langle\phi^2(0)\rangle_T\rangle^2 = \langle\phi^2(0)\rangle^2 \quad \text{(E10)}$$

$$\langle\langle\phi^2(0)\rangle_T^2\rangle = 2\langle\phi^2(0)\rangle^2 \quad \text{(E11)}$$

Thus subtracting $\langle\langle\phi^2(0)\rangle_T\rangle^2$ in the operation corresponding to the second equality of eq E8 gives an expression corresponding to eq D10. (It is also straightforward to show that $\langle\langle\phi^2(t)\phi^2(0)\rangle_T\rangle = \langle\phi^2(t)\phi^2(0)\rangle^0$ of eq D10.) The quantity $\langle\phi^2(0)\rangle_T$ is constant (proportional to the oscillator energy) in a given dynamical simulation of an oscillator. In eq E10 there is cancellation of the fluctuations in $\langle\phi^2(0)\rangle_T$ when averaging over an ensemble of oscillators with different energies; this cancellation is absent in eq E11, and the larger value results.

References

Adelman, S. A., & Doll, J. D. (1977) *Acc. Chem. Res. 10*, 378–384.

Bauer, D. R., Alms, G. R., Brauman, J. I., & Pecora, R. (1974) *J. Chem. Phys. 61*, 2255–2261.

Berne, B. J., Ed. (1977) *Modern Theoretical Chemistry*, Vol. 6, Plenum Press, New York.

Berne, B. J., & Pecora, R. (1976) *Dynamic Light Scattering*, Chapter 7, Wiley, New York.

Careri, G., Fasella, P., & Gratton, E. (1975) *CRC Crit. Rev. Biochem. 3*, 141–164.

Chandler, D. (1974a) *Acc. Chem. Res. 7*, 246–251.

Chandler, D. (1974b) *J. Chem. Phys. 60*, 3500–3507.
Chandrasekhar, S. (1943) *Rev. Mod. Phys. 15*, 1–89.
Chothia, C., Levitt, M., & Richardson, D. (1977) *Proc. Natl. Acad. Sci. U.S.A. 74*, 4130–4134.
Citri, N. (1973) *Adv. Enzymol. Relat. Areas Mol. Biol. 37*, 397–630.
Cooper, A. (1976) *Proc. Natl. Acad. Sci. U.S.A. 73*, 2740–2741.
Deisenhofer, J., & Steigemann, W. (1975) *Acta Crystallogr., Sect. B 31*, 238–250.
Del Rio, F., & DeLonngi, D. A. (1976) *Phys. Lett. A 56*, 463–464.
Deutch, J. M., & Silbey, R. (1971) *Phys. Rev. A 3*, 2049–2050.
Dickey, J. M., & Paskin, A. (1969) *Phys. Rev. 188*, 1407–1418.
Edsall, J. T. (1968) in *Structural Chemistry and Molecular Biology* (Rich, A., & Davidson, N., Eds.) pp 88–97, W. H. Freeman, San Francisco, CA.
Enskog, D. (1922) *K. Sven. Vetenskapsakad. Handl. 63 (4)*. Reprinted in *Kinetic Theory* (Brush, S. G., Ed.) Vol. 3, Pergamon Press, Oxford, 1972.
Fischer, S. F., & Laubereau, A. (1975) *Chem. Phys. Lett. 35*, 6–12.
Gear, C. W. (1966) Argonne National Laboratory Report No. ANL-7126.
Gear, C. W. (1971) *Numerical Initial Value Problems in Ordinary Differential Equations*, Prentice-Hall, Englewood Cliffs, NJ.
Gelin, B. R., & Karplus, M. (1975) *Proc. Natl. Acad. Sci. U.S.A. 72*, 2002–2006.
Gelin, B. R., & Karplus, M. (1977) *Proc. Natl. Acad. Sci. U.S.A. 81*, 801–805.
Gordon, R. (1966) *J. Chem. Phys. 44*, 1830–1836.
Hansen, J. P., & Klein, M. L. (1976) *Phys. Rev. B 13*, 878–887.
Hill, T. L. (1960) *An Introduction to Statistical Thermodynamics*, Addison-Wesley, Reading, MA.
Hodgkin, D. C., & Riley, D. P. (1968) in *Structural Chemistry and Molecular Biology* (Rich, A., & Davidson, N., Eds.) pp 15–28, W. H. Freeman, San Francisco, CA.
Honig, B., Ray, A., & Levinthal, C. (1976) *Proc. Natl. Acad. Sci. U.S.A. 73*, 1974–1978.
Huber, R., Kukla, D., Ruhlmann, A., Epp, O., & Formanek, H. (1970) *Naturwissenschaften 57*, 389–392.
Hynes, J. T. (1977) *Annu. Rev. Phys. Chem. 28*, 301–322.
Jencks, W. P. (1975) *Adv. Enzymol. Relat. Areas Mol. Biol. 43*, 219–410.
Karplus, M., Porter, R. N., & Sharma, R. (1965) *J. Chem. Phys. 43*, 3259–3287.
Kramers, H. A. (1940) *Physica (Utrecht) 7*, 284–304.
Levitt, M. (1974) *J. Mol. Biol. 82*, 393–420.
Litovitz, T. A. (1957) *J. Chem. Phys. 26*, 469–473.
Lowden, L. J., & Chandler, D. (1975) *J. Chem. Phys. 61*, 5228–5241.
Maradudin, A. A., Montroll, E. W., Weiss, G. H., & Ipatova, I. P. (1971) *Theory of Lattice Dynamics in the Harmonic Approximation*, Academic Press, New York.
McCammon, J. A., & Wolynes, P. G. (1977) *J. Chem. Phys. 66*, 1452–1456.
McCammon, J. A., Gelin, B. R., Karplus, M., & Wolynes, P. G. (1976) *Nature (London) 262*, 325–326.
McCammon, J. A., Gelin, B. R., & Karplus, M. (1977) *Nature (London) 267*, 585–590.
Narten, A. H. (1977) *J. Chem. Phys. 67*, 2102–2108.
Parzen, E. (1962) *Stochastic Processes*, Holden-Day, San Francisco, CA.
Pauling, L., Corey, R. B., & Branson, H. B. (1951) *Proc. Natl. Acad. Sci. U.S.A. 37*, 205.
Platz, O., & Gordon, R. G. (1973) *Phys. Rev. Lett. 30*, 264–267.
Ramachandran, G. N., Ramakrishnan, C., & Sasisekharan, V. (1963) *J. Mol. Biol. 7*, 95–99.
Richards, F. M. (1977) *Annu. Rev. Biophys. Bioeng. 6*, 151–176.
Rubin, R. J. (1972) *J. Chem. Phys. 57*, 312–316.
Schaeffer, H. F., III (1972) *The Electronic Structure of Atoms and Molecules*, Addison-Wesley, Reading, MA.
Schomaker, V., Waser, J., Marsh, R. E., & Bergman, G. (1959) *Acta Crystallogr. 12*, 600–604.
Slater, J. C., & Kirkwood, J. G. (1931) *Phys. Rev. 37*, 682–686.
Stark, R. E., Vold, R. L., & Vold, R. R. (1977) *Chem. Phys. 20*, 337–345.
Suezaki, Y., & Gō, N. (1975) *Int. J. Pept. Protein Res. 7*, 333–341.
Warme, P. K., & Scheraga, H. A. (1974) *Biochemistry 13*, 757–767.
Weber, G. (1975) *Adv. Protein Chem. 29*, 1–83.
Wilson, E. B., Jr., Decius, J. C., & Cross, P. C. (1955) *Molecular Vibrations*, McGraw-Hill, New York.
Zwanzig, R. (1965) *Annu. Rev. Phys. Chem. 16*, 67–102.
Zwanzig, R., & Ailawadi, N. K. (1969) *Phys. Rev. 182*, 280–283.